Chapter 8
Radio and Network Planning

Fernando J. Velez, Pedro Sebastião, Rui Costa, Daniel Robalo, Cláudio Comissário, António Rodrigues, and A. Hamid Aghvami

Abstract This chapter starts by presenting the Stanford University Interim (SUI) and modified Friis propagation models. Although the SUI model is being recommended for WiMAX, the comparison between the model and experimental results show that, in our environment, at 3.5 GHz, the modified Friis model with $g = 3$ fits better the measurement values. From the analyses of the signal-to-noise-plus-interference ratio, SNIR, interference-to-noise ratio and reuse pattern, it is found that both noise and interference present a strong limitation to the performance of fixed WiMAX, mainly for higher order modulation and coding schemes (MCSs). In general terms, the use of sectorization in fixed WiMAX enables to reduce the reuse pattern while considering sub-channelisation allows for improvement on the coverage. The reduction of the reuse pattern directly corresponds to an increase in the system capacity but the improvement in the coverage range (through sub-channelisation) can also allow for an improvement in UL system capacity, as adaptive MCS are used. Two different approaches are considered for graphical cellular planning, and the district of Covilhã is considered as a case study. On the one hand, one considered a GIS based WiMAX planning tool conceived by considering coverage issues, frequency reuse, and the impact of the different classes of service. On the other, Winprop^{TM} is used as it distinguishes among different MCS in the graphical presentation of the results. Both tools consider the information coming from the digital terrain profile. The GIS functionalities allow for appropriately adjusting azimuth and tilt of antennas. This cellular planning exercises confirm the results of theoretical analysis, where different crowns are achieved for the coverage with each MCS (corresponding to a given range of values for SNIR), for the maximum physical throughput, and for the "best server" cells. The frequency radio resources should be considered as the most valuable resource

F.J. Velez (✉)
Instituto de Telecomunicações-DEM, Universidade da Beira Interior, Calçada Fonte do Lameiro, 6201-001, Covilhã, Portugal
e-mail: fjv@ubi.pt

R. Prasad and F.J. Velez, *WiMAX Networks*,
DOI 10.1007/978-90-481-8752-2_8,

during the planning of wireless broadband access networks. As a rule, spectral efficiency needs to be optimized by using several advanced techniques, corresponding to an optimization from the cost-benefit point of view.

8.1 Introduction

The present context of frequency spectrum management worldwide, as well as the need for making broadband access flexible for users, creates opportunities for the entrance of new operators and offer diversification of innovative access technologies. As Worldwide Interoperability for Microwave Access (WiMAX) enables the support of mobile broadband Internet services in outdoor (and even in indoor, for the lower frequency bands) with high coverage ranges and user mobility support. It allows the exchange of truly wide and broadband multimedia content, and support simultaneously all-Internet Protocol (IP) voice, data, streaming, image and video multi-rate communications.

The goal of cellular coverage is to provide access to mobile users in a given region, called cell, while guaranteeing the quality of the received signal in both directions, Uplink (UL) and Downlink (DL), even for the users at the cell edge. As resources, for example, frequency channels, need to be reused in different geographical zones (but not in close proximity), the impact of interference among co-channel cells needs to be evaluated also in both directions. In WiMAX, as in Wideband Code Division Multiple Access (WCDMA) and High Speed Downlink Packet Access (HSDPA), the ideal situation would be to reuse the channels in every cell, that is, to deploy systems with a frequency reuse pattern, K, equal to one, which would be achieved by means of Pseudo Random Mapping (PRM) of sub-carriers where Orthogonal Frequency Division Multiple Access (OFDMA) is used. However, due to heavy interference in frequency reuse deployment, users at cell edge may suffer from low connection quality since these improvements may not be available in some versions of the standard, or may simply reduce but not eliminate the interference.

In the context of WiMAX planning, research on the variation of the carrier-to-noise-plus-interference ratio (*CNIR*) with different system parameters is therefore of paramount importance. As there are limitations in both links, UL and DL, techniques such as sub-channelisation need to be applied to reduce the impact of the noise on the link performance. However, only mobile WiMAX will allow for sub-channelisation in the DL while fixed WiMAX only allows for it in the UL, and may cause a degradation of performance (mainly owing to the extra noise caused by the largest bandwidth).

For cellular planning purposes, the UL and DL *CNIR*s from/at the wireless Subscriber Station (SS) are very important parameters. From a detailed analysis of its variation with the coverage and reuse distances for different modulation and coding schemes (MCS), an evaluation of the possible reuse patterns can be performed.

If Frequency Division Duplexing (FDD) is used, in fixed WiMAX, worst-case situations occur in the DL when the Base Station (BS) of the central cell transmits to the most distant SS, located at the cell edge, whilst receiving interference from the BS of the six co-channel cells of each ring of interference (Fig. 8.1). In the UL, the worst-case situation occurs when the SS is transmitting to the BS from the cell boundary while interfering mobiles are at the interfering cells edge (in the region closest to the central cell) (Fig. 8.2). When sectorization is considered the number of interfering cells is decreased, and system capacity increases.

Usage scenarios will be enabled by using innovative terminals, similar to PDAs or Tablet PCs, which will combine voice with other type of services, including image and video. One example can be the communication of real-time image from an actual fire site to the fire department. In Summer time, in the south of Europe, simultaneous fires in forests are a persistent calamity, and authorities lack access to real-time fire information in order to coordinate fire brigades. Another good example is the surveillance of commercial streets by using real-time video. For demonstration, a network was deployed in the city of Covilhã, Portugal, by using IEEE 802.16-2004 BreezeMAX Alvarion equipment with 3.5 MHz channels at 3.5 GHz [1], as indicated in Table 8.1 (where supported data rates are presented). Later, by using the IEEE 802.16e standard [2], it will be possible to support true mobility.

Different received power levels correspond to different net physical (PHY) bit rates, and to different modulation and coding schemes (MCSs), as shown in Table 8.2 (for the Alvarion BreezeMAX 3.5 MHz equipment).

This Point-to-Multipoint (PtM) network is the basic tool for our research inbroadband mobile access, mobile IP, and always best connected WiMAX scenarios, including the possibility of performing extensive field trials in the FDD mode. In the initial phase of WiMAX deployment, the operators experience is limited, and measurement based cellular planning procedures, extracted from the experimental

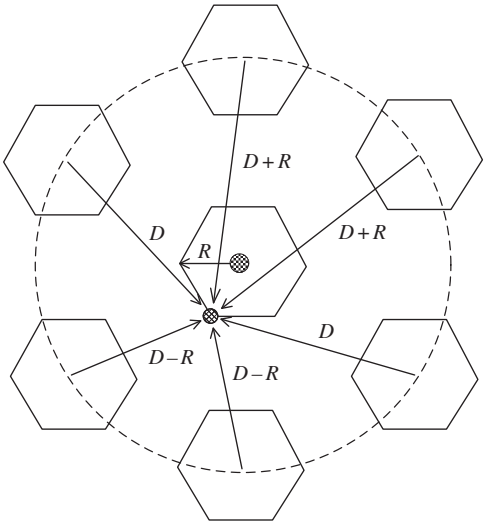

Fig. 8.1 Co-channel interference in the worst-case for the DL

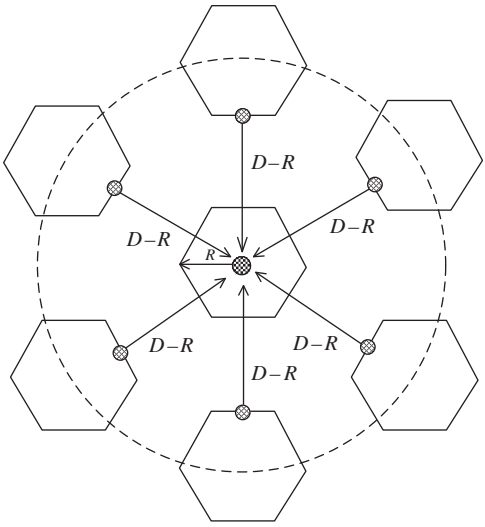

Fig. 8.2 Co-channel interference in the worst-case for the UL

Table 8.1 Total data rates for IEEE 802.16-2004

Bandwidth (MHz)	Data rate (Mbps)		
	QPSK	16-QAM	64-QAM
3.5	3.3	6.5	9.8
5.0	4.6	9.3	13.9
7.0	6.5	13.1	19.6
10.0	9.3	18.7	28.0
20.0	18.7	37.5	56.2

Table 8.2 Correspondence among modulations, sensitivity, and net PHY rate

Modulation & coding	Net PHY bit rate (Mbps)	Sensitivity (dBm)
BPSK 1/2	1.41	−100
BPSK 3/4	2.12	−98
QPSK 1/2	2.82	−97
QPSK 3/4	4.23	−94
QAM 16 1/2	5.64	−91
QAM 16 3/4	8.47	−88
QAM 64 2/3	11.29	−83
QAM 64 3/4	12.27	−82

networks and prototypes, are fundamental at for the validation of the proposed planning algorithms.

A Geographic Information Systems (GIS) based planning tool was developed for the purpose of helping in the process of design WIMAX coverage and frequency reuse. It includes the propagation models, the co-channel interference computation aspects, as well as the services and applications details. However, it does not fully includes a detailed analysis of the consequences of using different MCS, and a

comparison with a commercially available planning tool, as Winprop™ [3] was justified. This specific functionality of Winprop™ allows for helping to verify the impact of the improvement strategies, as sub-channelisation and sectorization. Different operation "modes" and the information coming from the digital terrain profiles will be considered in the context of specific cellular planning exercises.

The structure of this Chapter is as follows. Section 8.2 presents the point-to-multi-point propagation measurements and models, namely the modified Friis and the Stanford University Interim (SUI) models. Section 8.3 addresses aspects of cellular planning. It starts by discussing the limitations of a simplified analysis, and then a comparison of the results for the interference-to-noise ratio and the achievable reuse pattern is performed. The variation of the CNIR with co-channel reuse factor is used as a basis to compute the supported PHY throughput for different cases (by considering the absence and presence of sub-channelisation and of sectorization). Section 8.4 presents results obtained by using two wireless planning tool platforms, one developed by ourselves while the other one is commercially available. The framework and scenarios are analysed, the functionalities and potentials of the tools are discussed, and planning results are given for different environments as well. Finally, in Section 8.5 conclusions are made as well as suggestions for further work.

8.2 Propagation Models

8.2.1 SUI Versus Modified Friis Model

In Non Line-of-Sight (NLoS) channel conditions, signals may undergo scattering, diffraction, polarization changes and reflection impairments, which affect their level and phase at the receiver. Usually these impairments are not important if there is Line-of-Sight (LoS) between the transmitter and the receiver. For outdoor environments, obstacles, such as building materials, foliage and clutter, also contribute to increase path loss [4, 5], and the SUI outdoor propagation model is especially relevant [4]. It will be considered together with the modified Friis model.

Over the years, various models have been developed to characterize Radio Frequency (RF) environments and allow for the prediction of the RF signal strengths. These empirical models are used to predict large-scale coverage for radio communications systems in cellular applications and provide estimates for path loss (PL) by considering the distance between the transmitter and receiver, terrain factors, antenna height, and cellular frequencies. Nevertheless, according to [4] none of these approaches address the needs of broadband fixed wireless adequately. To overcome this limitation, AT&T developed an empirical wireless model that has been validated against deployed fixed wireless systems which yielded results comparable to other models and experiments. This model was the

basis of an industry-accepted model, and is being used by the standardization bodies, such as in the IEEE 802.16. The adoption of the AT&T wireless PL model by IEEE is referred as "Channel Models for Fixed Wireless Applications" in [5]. The AT&T wireless PL model includes, as parameters, antenna heights, carrier frequency and types of terrain [4]. Apart from the modified Friis model (where the propagation exponent γ instead of taking a value of 2 is replaced by a different empirical value), one possible solution for the Wireless Planning Tool (WPT) is therefore the SUI model, which is an extension of the earlier work of AT&T propagation model [4].

The SUI model uses three basic terrain types:

- Category A – Hilly/moderate-to-heavy tree density
- Category B – Hilly/light tree density or flat/moderate-to-heavy tree density
- Category C – Flat/light tree density

These terrain categories provide a simple method to estimate more accurately the PL of the RF channel in an NLoS situation. Being statistical in nature, the model is able to represent the range of PLs experienced within an actual RF link. SUI models were explored for the design, development, and testing of WiMAX links in six different scenarios, SUI-1 to SUI-6 [6]. By using these propagation models (both modified Friis and SUI ones), it is then possible to predict more accurately the coverage probability achieved within a base station site sector. These models do not replace detailed site planning (and site surveying), but can provide an estimate before actual planning. Besides, it is very important to perform RF planning activities to adequately evaluate specific environment factors, co-channel interference, actual clutter and terrain effects.

This model allows several frequencies and SSs heights. The path loss is given (in dB) by [7]

$$PL(d) = \overline{PL}(d_0) + 10 \cdot \gamma \cdot \log(d/d_0) + X_f + X_h + S, \tag{8.1}$$

with the following parameters

$$\overline{PL}(d_0)_{[dB]} = 20 \cdot \log(4\pi d_0/\lambda), \tag{8.2}$$

and

$$\gamma = a - b \cdot h_b + c/h_b, \tag{8.3}$$

where d is the distance between the BS and a given point, in meter, $d_0 = 100$ m, $\lambda = c/f$ is the wave length, $c = 3 \times 10^8 \mathrm{ms}^{-1}$, f is the carrier frequency, h_b is the BS height above ground, in meter ($10 < h_b < 80$ m), and a, b, and c are parameters which are chosen according to three environments, represented by A, B or C, Table 8.3. The terms X_f and X_h are correction factors for frequency and SS antenna height above the ground, respectively.

Table 8.3 Values for the parameters in the SUI model

Model constant	Terrain type		
	A	B	C
a	4.6	4.0	3.6
b	0.0075	0.0065	0.0050
c	12.6	17.1	20

These correction factors are defined as

$$X_f = 6.0 \cdot \log\left(f/2000\right), \tag{8.4}$$

and

$$X_h = \begin{cases} -10.8 \cdot \log\left(h_m/2.0\right), & \text{for terrain types A and B} \\ -20.0 \cdot \log\left(h_m/2.0\right), & \text{for terrain type C} \end{cases}, \tag{8.5}$$

where f is the carrier frequency, in MHz, and h_m is the receiver height above the ground, in meter. The term S is a lognormal-distributed random variable with zero mean and standard deviation σ_S, with typical values from 8.2 to 10.6 dB, depending on the type of terrain [7]. This term takes shadow fading originated by trees and structures into account [7].

The average received power is given by $\overline{PR}(d) = \overline{PE} - \overline{PL}(d)$, where $\overline{PE}$ is the average transmission power and $\overline{PL}(d)$ is the average path loss (attenuation factor).

In the context of other commercially available cellular planning tools, models with high complexity can be used, namely, the NLoS dominant ray path loss one [7, 8]. However, in order to obtain the most efficient cellular planning tools it is important to compare these models with the simplest ones, for example, the modified Friis and SUI ones, and validate them against experimental results.

8.2.2 Experimental Results

Figure 8.3 presents some of the PtM Alvarion WiMAX equipment used in the experimental setup installed on the roof top of the Health Sciences Faculty (HSF) of University of Beira Interior, Covilhã, near the Hospital. They are a BreezeMAX 3000 OFDM micro BS and self-installable Alvarion BreezeMAX Customer Premise Equipments (CPEs) operating at 3.5 GHz, an omnidirectional antenna, and the Outdoor Unit (ODU). The appropriate Ethernet and RF cables were also used, as well as a Global Positioning System (GPS) device, a 12–240 V power inverter (to feed the CPE), and a portable PC, used as a terminal and running a File Transfer

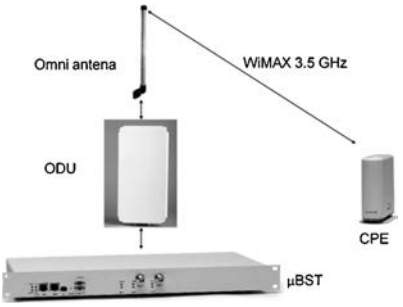

Fig. 8.3 IEEE 802.16-2004 PtM equipment operating at the 3.5 GHz band

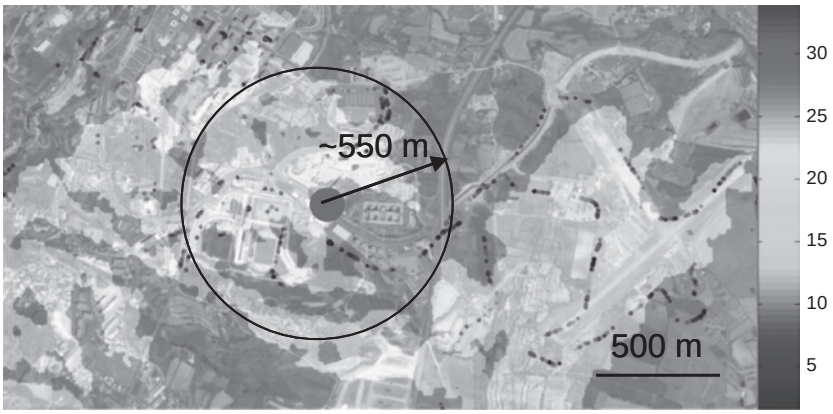

Fig. 8.4 LoS regions and measurements of $SNR_{[dB]}$ for the DL at 3.5 GHz

Protocol (FTP) application, the BreezeCONFIG software, and a tool for acquiring GPS positions. In the HSF backhaul network, there was an FTP server, and a Dynamic Host Configuration Protocol (DHCP) server, for automatically assigning an IP address to the users' CPEs. The BS antenna gain is 10 dBi (360° azimuth, 8° elevation, vertical polarization). The SS antenna is a beam switching array of six 9 dBi, 60° antennas, integrated into the CPE.

Field trials were performed in the suburban area of Covilhã, in a zone with approximately 2.80 × 1.55 km^2, and initial results for signal-to-noise ratio (SNR) and the throughput were obtained at the SSs (or CPEs) that roam around the suburban area surrounding the HSF. The dynamic range of the CPE was found to be adequate. There is a direct correspondence between the SNR values from Fig. 8.4, the MCSs, and the achieved data rate, for example, ∼6 Mbps for 16-QAM.

The BreezeMAX duplexing frequency range is 3,499.5–3,553.5 MHz and 3,550–3,600 MHz for downlink (DL), and 3,399.5–3,453.5 MHz, and 3,450–3,500 MHz for uplink (UL) [9]. In these particular field tests, our ODU was operating at 3,551.75 MHz (DL), and 3,451.75 MHz (UL), and with a transmitter power of 28 dBm. NLoS regions, obtained with ArcGIS, are also represented

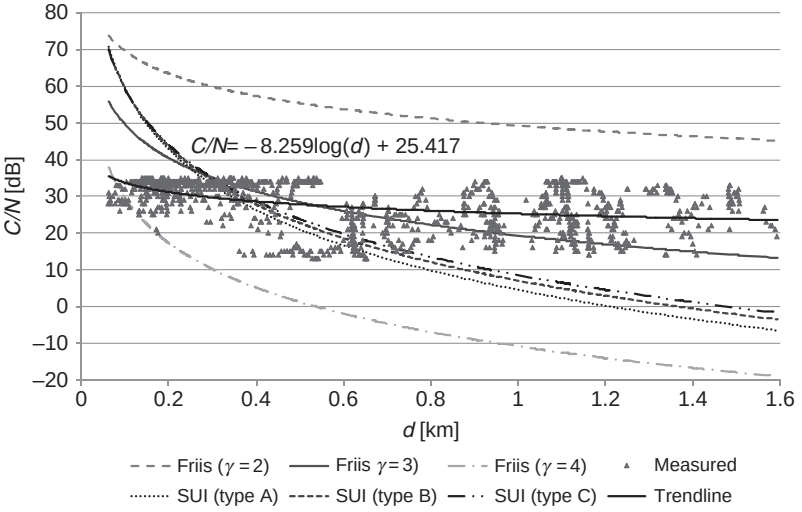

Fig. 8.5 Trend curve for the measured *SNR* in the locations around HSF: comparison between the SUI and the modified Friis models

in the background, in green, in Fig. 8.4. At distances far from the base station, the experimental regions with reasonable signal quality coincide basically with the LoS regions. However, for distances up to ∼550 m even NLoS areas near the boundary between LoS and NLoS areas can be covered.

Another important issue is the comparison between the results for the curve fitting of *SNR* and the curves obtained from the application of the propagation models (SUI model and modified Friis equation), as depicted in Fig. 8.5, for distances up to ∼1.6 km. Within the modified Friis model different propagation environments are modelled by different propagation exponents, γ, which vary from $\gamma = 2$, corresponding to free space conditions, for example, rural areas, to $\gamma = 3$, in urban areas (no shadowing), and $\gamma = 4$, in shadowed urban areas [10]. For the SUI model, one considers $h_m = 2$ m, $h_b = 13.3$ m and $\sigma_S = 8.8$ dB. For both models, a total antenna gain (transmitter plus receiver) of 19 dBi, a transmitter power of 28 dBm, a bandwidth of 3.5 MHz, and a noise factor of 3 dB were assumed.

To understand the results, an analysis of the terrain profile around the BS location at HSF is required. While at Southeast (SE) of the BS the terrain is flat, at Northwest (NW) it is continuously hilly, with increasing altitudes. The first coverage circular zone, with a radius of ∼550 m from the BS, is part of the suburban region of Covilhã, with a moderate building density.

The second coverage zone (or crown), for distances larger than 550 m, corresponds to a rural area (and the small airport) at Southeast, and to a dense urban area at NW. However, this dense urban area corresponds to zones predominantly in LoS with the BS as the terrain height continuously increases from the BS to this zone. At SE, the zones up to a distance of ∼550 m are predominantly in non-LoS owing to the shadowing effect of the HSF roof. However, at NW of the BS, this crown is

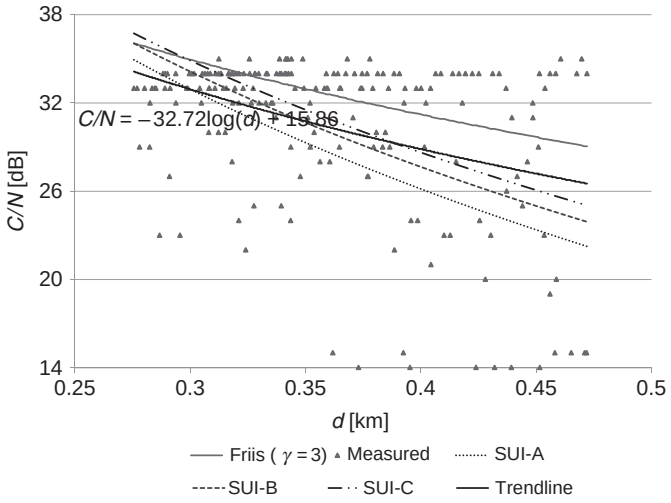

Fig. 8.6 Analysis of the measured *SNR* for distances in the interval [275, 475] m: comparison between the SUI and the modified Friis models

predominantly in LoS (as for higher distances), as the terrain height increases. For distances larger than 550 m measurements were taken mostly at locations with LoS coverage.

A curve fitting approach was used to interpret the measurement results from Fig. 8.5 (in dB). The coefficient -8.259 for $\log(d)$ corresponds to a very low power decay rate. If the modified Friis equation is considered, the experimental results take values similar with the curve for $\gamma = 4$ for distance in the interval (60, 150 m), similar to the ones from the curve for $\gamma = 3$ for distances in the interval (300, 500 m). Then, for larger coverage distances, values correspond to modified Friis equation propagation exponents between 2 and 3. It seems that the results consecutively correspond to (1) shadowed urban areas, (2) urban areas (with no shadowing), and (3) approximately free space, which is partially true if we consider the actual terrain.

Despite the fact that the use of the SUI model is being recommended for WiMAX, the comparison of the experimental results with the SUI model is harder since they only coincide for distances in the interval (275, 475 m). In order to clarify this issue, Fig. 8.6 presents a partial analysis of the results for *C*/*N* in this interval, where a different trendline is obtained, and only the modified Friis equation curve for $\gamma = 3$ is considered for comparison, as it approximately follows the experimental trendline for the results with a difference of circa 2.5 dB (which can be caused by the penetration loss due to the placement of the SS antenna in the rear seat of the car during the measurements). If this difference of 2.5 dB was subtracted from results for modified Friis equation with $\gamma = 3$, the curves would be almost coincident. This was confirmed by the reduction of the Mean Square Error (MSE) from 4.917 to 0.113.

Without this correction factor, while the distance to the BS increases the trend line consecutively crosses the curves for SUI-A, SUI-B, and SUI-C, that is, the curves for (a) hilly/moderate-to-heavy tree density, (b) hilly/light tree density or flat/moderate-to-heavy tree density, and (c) flat/light tree density, respectively.

The experimental results cross the three curves of the SUI model but a good correspondence was only found for the SUI-B and SUI-C, as the MSE are 1.564 and 1.617, respectively. For the SUI-A curve, the MSE was 4.657. However, if we apply the correction factor of 2.5 dB (as for the modified Friis equation) the results for the SUI-A and SUI-B models would be much worst (MSE of 19.227 and 9.247, respectively). Only the curve for the SUI-C would still offer an almost acceptable correspondence (with an MSE of 4.808).

Results from field trials show that, at 3.5 GHz, the propagation at distances higher than 550 m is mainly in LoS; hence, a need is identified of using lower frequency bands to achieve the objective of having appropriate NLoS propagation within WiMAX networks. Another important result at this band is the appropriateness of the modified Friis propagation model for this band. Despite the use of the SUI model is recommended for WiMAX, in these experiments at 3.5 GHz, for distances in the interval (275, 475 m), the experimental results fit quite well with the modified Friis equation with $\copyright \sim 3$, which corresponds to urban areas (with no shadowing), although the SUI-C model can also be a solution.

8.3 Cellular Planning

8.3.1 Limitations of a Simplified Analysis

In order to achieve an efficient use of the radio frequency spectrum, it is important to choose a frequency reuse scheme that leads to coverage guarantee, and improved system capacity whilst minimising the interference. If FDD is used, an analytical approach may be followed in fixed WiMAX (IEEE 802.16-2004) to solve coverage and frequency reuse problems. Traditionally, several text books decouple the analysis of the carrier-to-noise ratio aspects from the analysis of the carrier-to-interference ones. This way, interference is not considered in the coverage problem while noise is not considered when addressing the frequency reuse.

On the one hand, not considering the interference in the coverage problem means that the maximum coverage distance is obtained without allowing for extra margin for the interference, which is a critical limitation for the dimensioning process of a cellular system. On the other hand, the absence of noise in the interference analysis is unrealistic, as noise is always present in communications.

As there would be limitations arising from an independent analysis, cellular planning has to consider simultaneously carrier-to-noise and carrier-to-interference constraints. Improvement techniques as sub-channelisation and sectorization, will be addressed to improve coverage and avoid interference.

8.3.2 Signal-to-Noise-Plus-Interference Ratio

This Section addresses aspects related to the analysis of the cell coverage distance (or cell radius), R, the co-channel reuse factor, rcc, the ratio between the reuse and the coverage distances, the reuse pattern, K, for several levels of IEEE 802.16 modulation and coding schemes. The conclusions to be extracted facilitates an adequate choice of the reuse pattern and an efficient frequency planning.

If one considers the interference-to-noise ratio, defined by

$$M = {}^{I}/_{N}, \tag{8.6}$$

and the equation for the carrier-to-noise-plus-interference ratio (*CNIR*) to be used in the dimensioning process is

$$\frac{C}{(N+I)} = \left(\frac{C}{N}\right)_{\min}, \tag{8.7}$$

Equation (8.7) can therefore be re-written in the two following ways

$$\frac{C}{N} = \left(\frac{C}{N}\right)_{\min}(1+M), \tag{8.8}$$

and

$$\frac{C}{I} = \left(\frac{C}{N}\right)_{\min}\left(1+M^{-1}\right). \tag{8.9}$$

In (8.7) one is using the model for *CNIR* from [11] while assuming that the weights for noise and interference are the same.

From Eq. (8.8) one obtain the following equation for the interference-to-noise ratio

$$M(R) = \frac{(C(R)/N)}{(C/N)_{\min}} - 1, \tag{8.10}$$

where $C(R) = P_R(R)$ is computed by applying the modified Friis formula with $\gamma = 3$, the hypothesis followed in this Section for urban environments. This value for the propagation exponent results from the experimental results in Covilhã, Portugal.

Values of $M(R)$ are proportional to the interference still tolerable for a given coverage distance R while (still) agreeing with the quality requirements for a given MCS.

With a hexagonal cell topology, in the DL (Fig. 8.1) as the distance associated with interference is D, that is, the reuse distance itself, the carrier-to-interference ratio can be given by

$$\frac{C}{I} = \frac{1}{2(r_{cc}+1)^{-\gamma} + 2{r_{cc}}^{-\gamma} + 2(r_{cc}-1)^{-\gamma}} \approx \frac{{r_{cc}}^{\gamma}}{6}, \tag{8.11}$$

where r_{cc} is the co-channel reuse factor, given by

$$r_{cc} = {}^{D}\!/_{R}. \tag{8.12}$$

The approximate expression in (8.11) is very useful in practice.

For the UL (Fig. 8.2) the carrier-to-interference ratio is given by

$$\frac{C}{I} = \frac{(r_{cc}-1)^{\gamma}}{6}. \tag{8.13}$$

By replacing (8.11) into (8.9), it is therefore possible to obtain the following equation for the reuse factor in the DL

$$r_{cc} = \sqrt[\gamma]{6 \cdot (1+M^{-1}) \cdot \left({}^{C}\!/_{N}\right)_{\min}}. \tag{8.14}$$

For the UL, in turn, by replacing (8.13) into (8.9), one obtain the following equation

$$r_{cc} = \sqrt[\gamma]{6 \cdot (1+M^{-1}) \cdot \left({}^{C}\!/_{N}\right)_{\min}} + 1. \tag{8.15}$$

It is worthwhile to note that, for hexagonal reuse geometries, the reuse pattern is given by

$$K = \frac{{r_{cc}}^{2}}{3}. \tag{8.16}$$

As a horizontal asymptote arises in the analysis of the curves of r_{cc} as a function of the coverage distance, R, it is important to present the mathematical details associated to it.

To compute the horizontal asymptote in the chart of $r_{cc}(R)$, one has to consider that $R \to 0$. From (8.10), if $R \to 0$ then $M \to +\infty$, and $M^{-1} \to 0$. On the one hand, for the DL, in the limit, one obtains

$$\lim_{R \to 0} r_{cc} = \sqrt[\gamma]{6 \cdot \left({}^{C}\!/_{N}\right)_{\min}}. \tag{8.17}$$

On the other, for the UL, also in the limit, one obtains

$$\lim_{R\to 0} r_{cc} = \sqrt[\gamma]{6 \cdot \left(C/N\right)_{\min}} + 1. \tag{8.18}$$

By considering (8.16), it is straightforward to conclude that, for each value for the propagation exponent, the reuse pattern, K, only depends on the MCS through the value of the corresponding minimum carrier-to-noise ratio, as well as on the cellular interference geometry, either UL or DL.

While the asymptotic reuse factor is associated with the upper bound for system capacity, the maximum coverage distance is associated with the carrier-to-interference-plus-noise ratio at the cell boundary when the interference is null. Since the interference-to-noise ratio, M, represents the interference that can still be tolerated for a given R, in the limit, the maximum coverage distance for which no extra interference is tolerated is obtained when $I(R) \to 0$, that is, when $M(R) \to 0$ (meaning that $M_{[\mathrm{dB}]} \to -\infty$). Hence, the vertical asymptotes for the $M(R)$ and $r_{cc}(R)$ charts is

$$R_{asymptote} = R_{M\to 0}. \tag{8.19}$$

It is obtained by solving the following equation

$$M(R) = \frac{(C(R)/N)}{(C/N)_{\min}} - 1 = 0, \tag{8.20}$$

or, in a simplified way

$$C(R)/N = \left(C/N\right)_{\min}. \tag{8.21}$$

By comparing this equation (valid only when $M \to 0$) with Equation (8.8), one concludes that only considering the carrier-to-noise ratio to determine the coverage distance, R, is inadequate in systems where interference is relevant, as Equation (8.21) corresponds to a null interference-to-noise ratio, M. If a cellular system was dimensioned this way there would not be an extra margin for interference, represented by $M = I/N$. Finally, it is a worth noting that, for a given propagation exponent, the maximum coverage distance corresponding to the vertical asymptote, $R_{\mathrm{asymptote}}$, depends not only on the MCS but also on the noise power, N. This is the reason why the reduction of the noise power through sub-channelisation, that is, through the reduction of the RF bandwidth, is so important.

8.3.3 Interference-to-Noise Ratio and Reuse Pattern

By using (8.10), one obtains the chart for the interference-to-noise ratio without sub-channelisation from Fig. 8.7, which is valid both for the UL and DL. The considered propagation exponent for the modified Friis model is $\gamma = 3$.

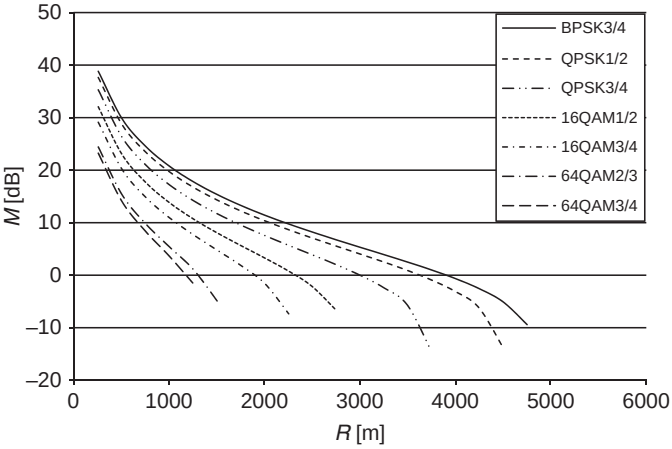

Fig. 8.7 Interference-to-noise ratio without sub-channelisation

Table 8.4 Values for the vertical asymptote without sub-channelisation

Level	MCS	$R_{asymptote}$ (m)
1	BPSK 1/2	5,814.86
2	BPSK 3/4	4,911.41
3	QPSK 1/2	4,548.55
4	QPSK 3/4	3,783.32
5	16-QAM 1/2	2,936.79
6	16-QAM 3/4	2,368.86
7	64-QAM 2/3	1,638.85
8	64-QAM 3/4	1,494.65

The modified Friis propagation model with $\gamma = 3$, transmitter power $P_t = -2$ dBW, and transmitter and receiver antenna gains $G_t = 17$ dBi and $G_r = 9$ dBi, respectively, were assumed. Note that transmitter antenna gain is 7 dB higher than the value considered in Section 8.2.2. The radio frequency bandwidth, the noise figure and the frequency were $b_{rf} = 3.5$ MHz, $N_f = 3$ [dB], and $f = 3.5$ GHz, respectively. Table 8.4 presents the corresponding values for the vertical asymptote without sub-channelisation, $R_{\text{asymptote}}$. It is observed a relevant decrease of the values for the vertical asymptote (maximum coverage distance) as the MCS level increases, which is compatible with the lowest values for $SNR_{\min}$.

By applying (8.14) and (8.16) to the DL one obtains the charts for $r_{cc}(R)$ and $K(R)$ from Figs. 8.8 and 8.9, respectively.

By using a reuse pattern $K = 7$ it is possible to use a maximum MCS level of 4, that is, QPSK , for $R \leqslant 2.7$ km, and a maximum MCS level of 5, that is, 16-QAM ½, for coverage distances lower than 1.2 km.

Figure 8.10 presents the results for the UL, which are worst since they correspond to higher values for the reuse pattern. In the UL without sub-channelisation, for a reuse pattern $K = 7$, only a low order MCS is achievable, that is, QPSK , up to a coverage distance of 2 km. It is not possible to use 16-QAM ½, as it was in the DL.

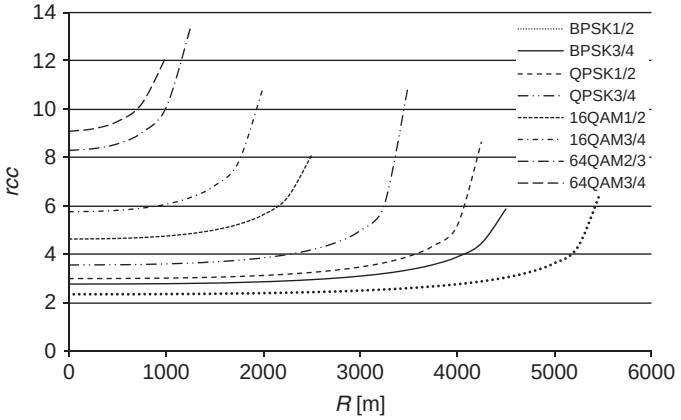

Fig. 8.8 Reuse co-channel factor as a function of the coverage distance with MCS level as a parameter, in the DL without sub-channelisation

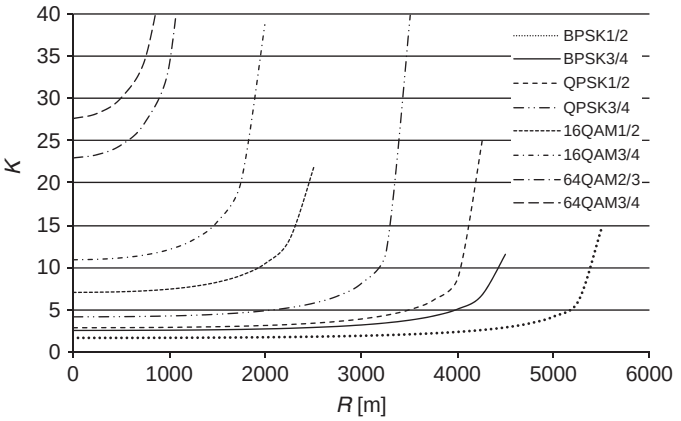

Fig. 8.9 Reuse pattern as a function of the coverage distance with MCS level as a parameter, in the DL without sub-channelisation

It is therefore important to address techniques for the improvement of system capacity and coverage range. As sub-channelisation in the IEEE 802.16-2004 UL is an optional feature, one explored its impact on the achieved MCS. Differently from the mobile version of WiMAX, IEEE 802.16-2004, based on Orthogonal Frequency division Multiplexing Physical (OFDM-PHY), does not support sub-channelisation in the DL. For the UL, the use of sub-channelisation limits the SS transmissions to 1/16 of the bandwidth assigned to the communication through the BS. The standard defines 16 sub-channels, and 1, 2, 4, 8 or all sets of sub-channels can be assigned to a SS, and each subscriber may use a different MCS in a more permanent way as far he/she is using a different sub-channel.

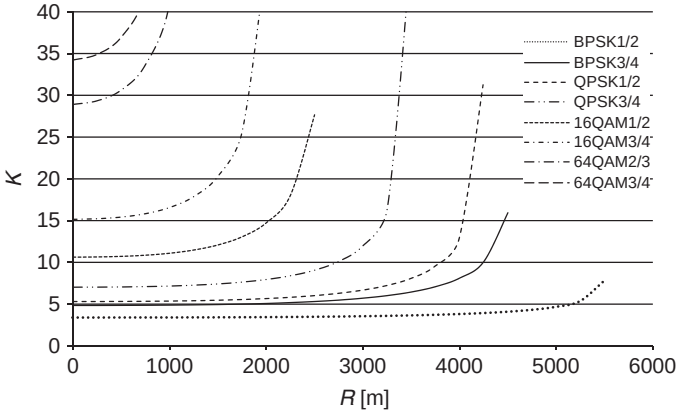

Fig. 8.10 Reuse pattern as a function of the coverage distance with MCS level as a parameter, in the UL without sub-channelisation

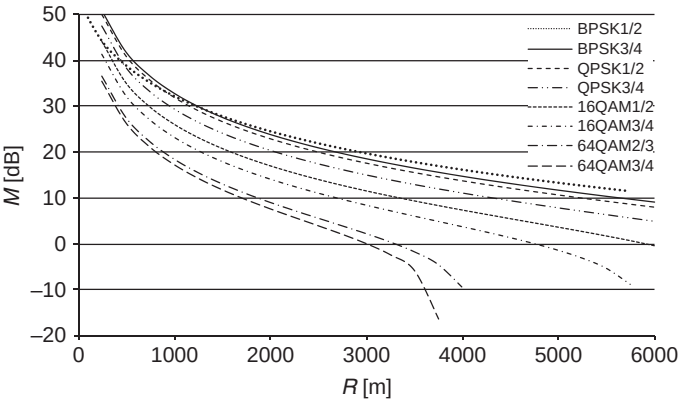

Fig. 8.11 Interference-to-noise ratio with sub-channelisation (valid for both links)

Nevertheless, in the DL, as the MCS can be chosen at burst level, there is also the flexibility of using different MCS by different users (even without sub-channelisation), as they use different consecutive bursts within a frame.

By using (8.10) and (8.15) one obtains the charts for M(R) and K(R) from Figs. 8.11 and 8.12, respectively. Table 8.5 presents the new values for the vertical asymptotes, which are clearly higher than the ones without sub-channelisation (more than twice the value). In this case, with 16 sub-channels, the variation of the noise power is $10 \cdot log(1/16) = -12$ dB, providing an enhancement of 12 dB in the link budget. By comparing the evolution of $K(R)$ from Fig. 8.12 with the case without sub-channelisation there is no decrease in the reuse pattern; as a consequence, there is no direct increase in system capacity for the lowest values of R (only the achievable coverage distances are increased). For $K = 7$, the achievable

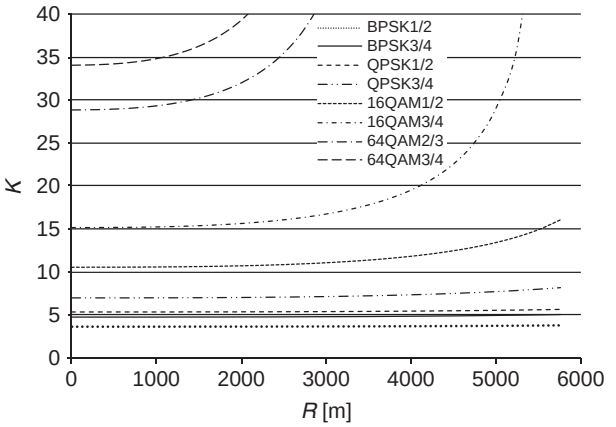

Fig. 8.12 Reuse co-channel pattern as a function of the coverage distance with MCS level as a parameter, in the UL with sub-channelisation

Table 8.5 Values for the vertical asymptote with sub-channelisation

Level	MCS	$R_{asymptote}$ (m)
1	BPSK 1/2	14,652.51
2	BPSK 3/4	12,375.98
3	QPSK 1/2	11,461.63
4	QPSK 3/4	9,533.36
5	16-QAM 1/2	7,400.25
6	16-QAM 3/4	5,969.16
7	64-QAM 2/3	4,129.65
8	64-QAM 3/4	3,766.28

MCS is QPSK . However, the achievable coverage distance increases from 2 to 5 km, approximately.

It is a worth noting that, in this case, the QPSK ½ MCS may be used up to a coverage distance of 6 km.

In order to achieve higher system capacity the use of sectorization is suggested. The use of 120° sectorial BS antennas is adopted, that is, one proposes the use of tri-sectorial antennas.

By inverting both members of (8.9) while using the formula for C/I from [12], one obtains

$$\left[(r_{cc}+0.7)^{-\gamma}+(r_{cc}-0.22)^{-\gamma}\right]-\frac{1}{(1+M^{-1})\cdot(C/N)_{\min}}=0, \tag{8.22}$$

which is valid both for UL and DL. The minimum reuse factor required for such a tri-sectorial system may be obtained by solving this equation in order to r_{cc} while obtaining the reuse pattern through the use of (8.16). Note that, for the omnidirectional case, the usual assumptions for interference coming from six sources of interference were used in the computations. Although one only have considered

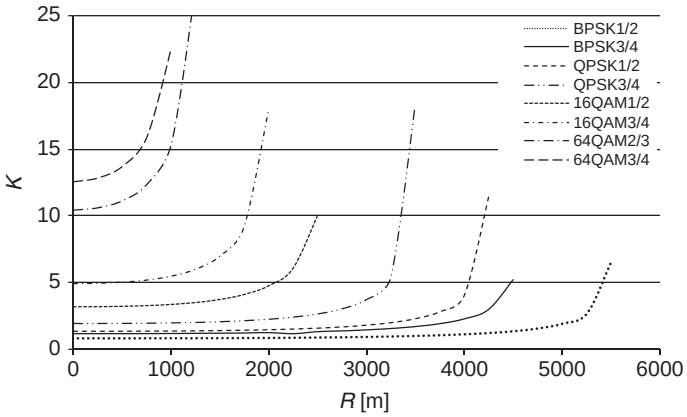

Fig. 8.13 Reuse pattern as a function of the coverage distance with MCS level as a parameter, in the UL with sectorisation but without sub-channelisation

one ring of interference some care would be needed if lower propagation exponents were used [11, 13].

Figure 8.13 presents the chart for the variation of the reuse pattern, K, with the coverage distance. As no sub-channelisation is considered in this case, the vertical asymptotes are the ones from Table 8.4.

It is observed that, with sectorization, a clear improvement is obtained in the reuse pattern results in comparison with the ones previously presented, as reuse patterns suffer an important reduction. For $K = 7$ it is now possible to consider level 6 MCS, that is, 16-QAM 3/4, up to $R \sim 1.5$ km, overcoming the level 5 MCS without sectorization. While 16-QAM 3/4 can be used for coverage distances up to 1.5 km, 16-QAM ½ may be used up to $R \sim 2.2$ km. With the QPSK ½ and QPSK 3/4 MCSs it is possible to achieve $K = 7$ for coverage distances up to approximately 4.1 and 3.3 km, respectively.

The use of sub-channelisation increases the coverage distance while the use of sectorization increases the achievable system capacity (through the decrease of the reuse pattern). It is therefore worthwhile to explore the simultaneous use of sub-channelisation and sectorization. Figure 8.14 presents the variation of the reuse pattern with the cell coverage distance for this new case, only possible in the UL for fixed WiMAX.

Larger coverage distances are possible together with lower reuse distances. With $K = 7$, it is possible to achieve the 16-QAM 3/4 MCS (level 6) up to $R = 4.3$ km, while the achievable MCS is 16-QAM ½ MCS (level 5) up to a coverage distance of 6.0 km.

In this case, with $K = 3$, lower order MCSs, for example, BPSK ½, BPSK 3/4, QPSK ½, or QPSK 3/4, are perfectly achieved up to coverage distances larger than 6.0 km.

The reduction of the reuse pattern directly corresponds to an increase in system capacity (but not in the cellular coverage). However, it indirectly contributes to an

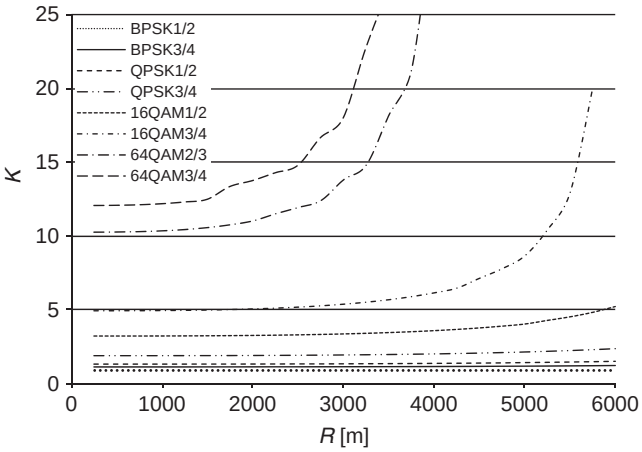

Fig. 8.14 Reuse pattern as a function of the coverage distance with MCS level as a parameter, for the UL, with the use of sectorisation and sub-channelisation

increase in system capacity as higher level MCSs are made available into outer cell coverage rings through the use of adaptive MCSs.

One issue that is left for further study is the dependence of these results on the propagation exponent, γ. For example, if the propagation exponent decreases the value of the coverage distance asymptote will increase but the asymptotic value for the reuse factor, r_{cc}, will also increase, corresponding to a reduction on the supported system capacity by each MCS.

8.3.4 CNIR and Supported Throughput

To better understand the changes caused by sub-channelisation (16 sub-channels) and sectorization it is worthwhile to plot the *CNIR* curves as a function of the reuse factor, r_{cc}, with R as a parameter. To produce these curves the power of the carrier is obtained by computing the power received by an SS at a distance R from the BS while the computation of the interference depends on the UL and DL configuration, and on the use of sectorization as well. It can be computed, for a fixed R, by making the same considerations for the reuse as assumed for Equations (8.11), (8.13) and (8.22). Although IEEE 802.16-2004 cannot use sub-channelisation in the DL, one important comparison is between absence and presence of sub-channelisation in the UL. Another important case is the simultaneous use of sub-channelisation and sectorization.

From these charts, considering C/N thresholds for each MCS, that is, $(C/N)_{\min}$, it is straightforward to obtain the achievable physical cell throughput, not considering the mixture of services and applications and the corresponding "multiplexing" characteristics. These charts allow for exploring what the achievable *CNIR* and

throughput are for a given reuse pattern, K. As, for hexagonal cells, $K = 7$ corresponds to a reuse factor $r_{cc} = 4.58$ this value is considered as a goal.

We are aware that, for the cases where sub-channelisation is considered in Fixed WiMAX, the approach we follow for *CNIR* does not cope with per sub-channel equivalent *SINR* (or *CNIR*) computations. These computations can be performed accounting either for exponential effective *SINR* mapping (EESM), effective code rate map (ECRM), or mean instantaneous capacity (MIC), and may be applied in the future to improve the relevance of the *CNIR* curves through the use of one of these compression techniques.

Figure 8.15 shows *CNIR* as a function of r_{cc} with R as a parameter for the UL while Fig. 8.16 presents the corresponding variation of the achievable physical throughput with r_{cc} for each MCS.

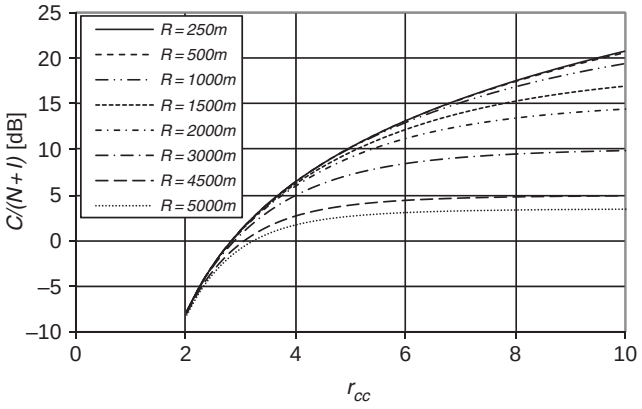

Fig. 8.15 *CNIR* as a function of r_{cc} with R as a parameter, in the UL, no sub-channelisation

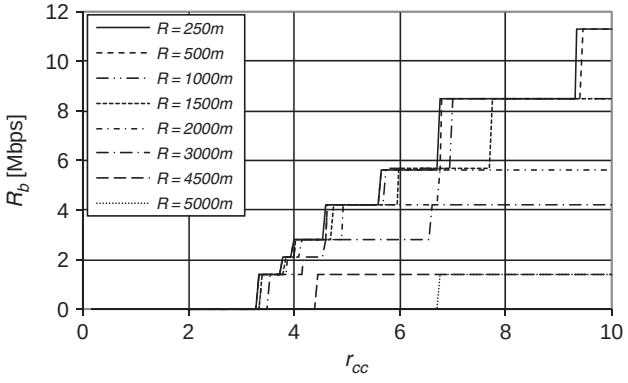

Fig. 8.16 Physical throughput as a function of r_{cc} with R as a parameter, in the UL, no sub-channelisation

It is clear that for $r_{cc} = 4.58$ values of *CNIR* are always lower than 8.9 dB while for coverage distances larger than 2 km it decreases drastically. As a consequence, for $r_{cc} = 4.58$, the achievable physical throughput is very low ($R_b = 2.82$ Mbps maximum) compared with the maximum achievable, that is, 12.27 Mbps, Fig. 8.16. For the DL the results are better, Fig. 8.17, and PHY throughput of 4.23 Mbps is achieved for distances up to 2 km.

Figures 8.18 and 8.19 present the results for *CNIR* and R_b as a function of r_{cc}, in the UL with sub-channelisation. Improvements are only evident for the longest coverage distances, that is, with sub-channelisation the main improvement is on the coverage. If sectorization is applied alone then the values for *CNIR* at $r_{cc} = 4.58$ will be higher. However, a truly improvement for coverage distances up to 3 km (not only 2 km anymore) requires both sectorization and sub-channelisation for the UL, as *CNIR* exceeds 15 dB, as shown in Figs. 8.20 and 8.21.

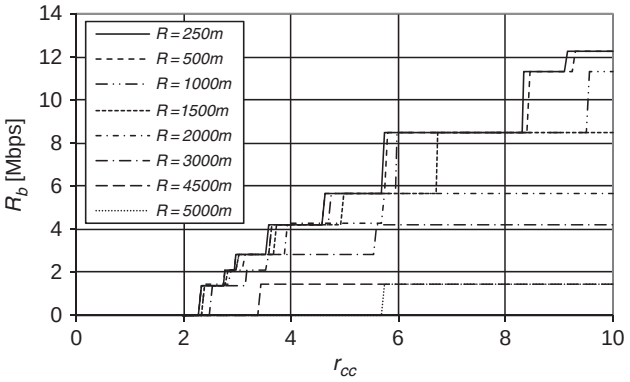

Fig. 8.17 Physical throughput as a function of r_{cc} with R as a parameter, in the DL

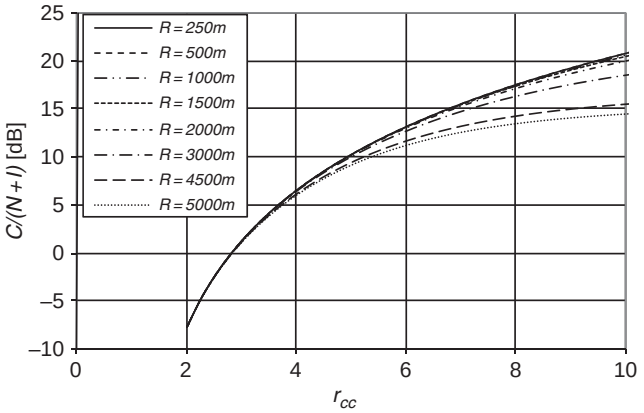

Fig. 8.18 *CNIR* as a function of r_{cc}, with R as a parameter, in the UL with sub-channelisation

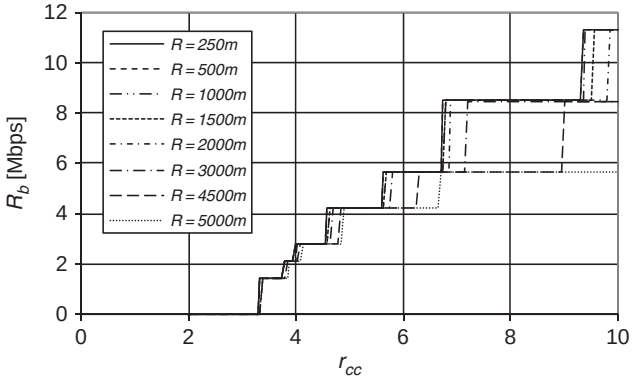

Fig. 8.19 Supported throughput as a function of r_{cc}, with R as a parameter, in the UL with sub-channelisation

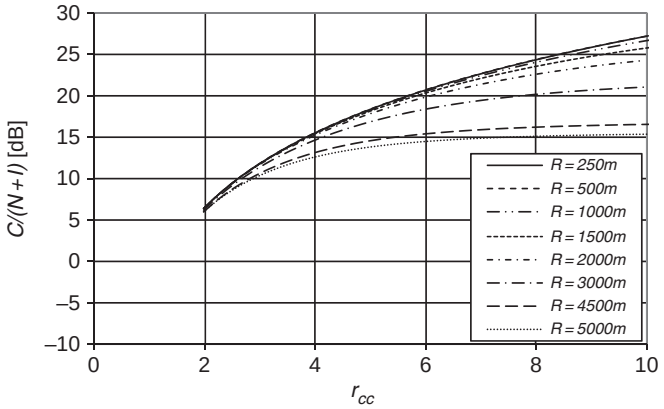

Fig. 8.20 *CNIR* as a function of r_{cc}, with R as a parameter, in the UL with sub-channelisation and sectorization

This leads to a clear confirmation of the need for the simultaneous use of both improvement techniques. Improvements in the analysis can be obtained with the assessment of the supported throughput, R_b, as a function of the distance within a cell when the coverage distance (or cell radius) takes a given value, for example, 2 or 3 km.

As, for a fixed r_{cc}, larger coverage distances imply coverage limitations but less interference, it is important to compare the achievable maximum throughput for a given reuse pattern, for example, $K = 7$, for each value of the distance, d (from the BS to an SS) and each MCS, for different Rs.

In the omnidirectional case, while the power of the received carrier is computed for a distance d, the distances assumed for the computation of co-channel

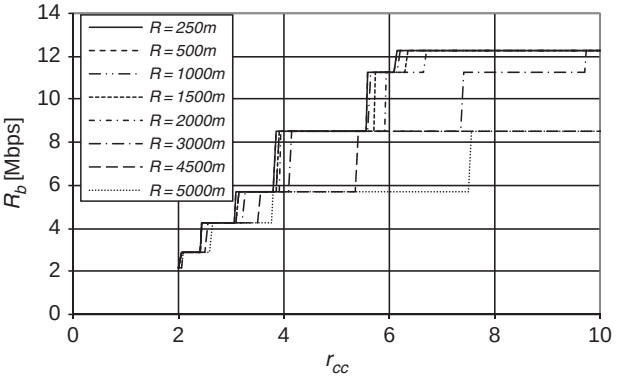

Fig. 8.21 Physical throughput as a function of r_{cc}, with R as a parameter, in the UL with sub-channelisation and sectorization

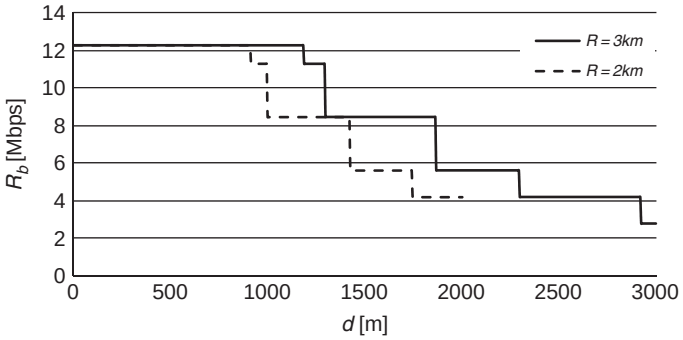

Fig. 8.22 Maximum achievable physical throughput as a function of d for $R = 2$ and 3 km, in the DL in the absence of sub-channelisation and sectorization ($K = 7$)

interference are maintained, that is, $r_{cc} \cdot (R - 1)$ in the UL and $\sim r_{cc} \cdot R$ in the DL. In the tri-sectorial case, the power of the received carrier is also computed for a distance d, whilst considering the following equation for co-channel interference

$$C/I = \frac{d^{-\gamma}}{(r_{cc} \cdot R + 0.7 \cdot d)^{-\gamma} + (r_{cc} \cdot R - 0.22 \cdot d)^{-\gamma}}, \tag{8.23}$$

Figure 8.22 shows the maximum achievable physical throughput as a function of d for $K = 7$ for the DL, in the absence of sub-channelisation and sectorization, while Fig. 8.23 presents the case of UL, and achieved results are worst.

Figure 8.24 shows the same type of results in the presence of sub-channelisation but without sectorization while Fig. 8.25 presents results in the absence of sub-channelisation and with sectorization. For a fixed K, with the use of sectorization

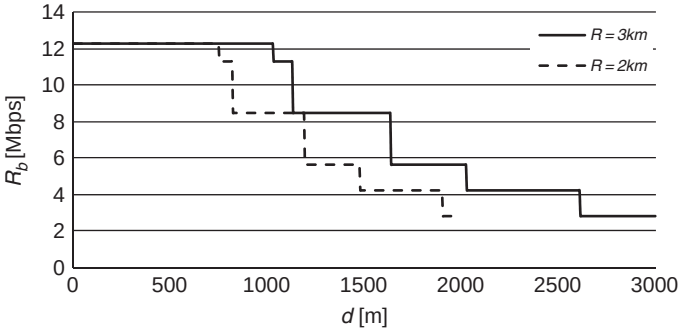

Fig. 8.23 Maximum achievable physical throughput as a function of d for $R = 2$ and 3 km, in the UL in the absence of sub-channelisation and sectorization ($K = 7$)

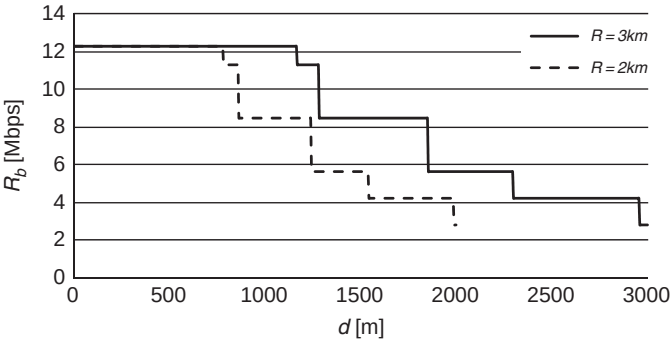

Fig. 8.24 Maximum achievable physical throughput as a function of d for $R = 2$ and 3 km, in the UL, with sub-channelisation but without sectorization ($K = 7$)

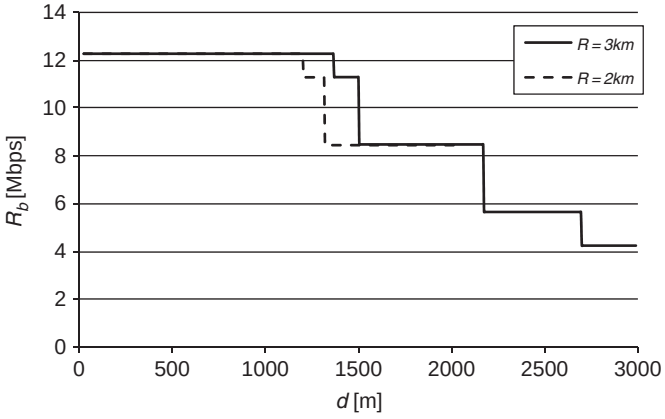

Fig. 8.25 Maximum achievable physical throughput as a function of d for $R = 2$ and 3 km, in the UL, without sub-channelisation but with sectorization ($K = 7$)

(tri-sectorial 120° antennas) it is visible a clear increase on the distances where the highest throughputs are achievable.

Figure 8.26 presents the case with the simultaneous use of sub-channelisation and sectorization (tri-sectorial 120° antennas).

Tables 8.6 through 8.8 present a summary of the values of the maximum distances up which the different MCS may be used (and the respective values of the physical throughput). By using these values for the distance, it is possible to obtain the area of the coverage rings where each MCS is supported in the absence of sectorization, Tables 8.9 and 8.10 (for $R = 2$ and 3 km, respectively), and with sectorization, Tables 8.11 and 8.12 (in the presence or absence of sub-channelisation, respectively). If one assumes a uniform distribution of users, the area of the coverage rings represents the percentage of use for each MCS.

For a fixed K, the use of sub-channelisation improves the coverage slightly but only sectorization clearly improves the results for the achievable physical throughput. Furthermore, the simultaneous use of sub-channelisation and sectorization clearly benefits the possibility of using the highest level MCSs for larger coverage distances (compared with the cases of absence of sub-channelisation and sectorization).

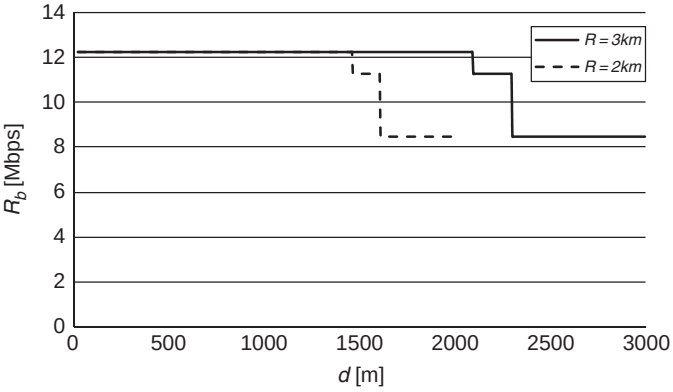

Fig. 8.26 Maximum achievable physical throughput as a function of d for $R = 2$ and 3 km, in the UL, with sub-channelisation and sectorization ($K = 7$)

Table 8.6 Achievable distance, d, versus supported physical throughput and MCS, for R = 2 and 3 km in the absence of sub-channelisation and sectorization

R_b (Mbps)	MCS	d (m)			
		$R = 2$ km		$R = 3$ km	
		DL	UL	DL	UL
12.27	64-QAM	910	750	1,185	1,030
11.29	64-QAM 2/3	995	820	1,295	1,130
8.47	16-QAM	1,420	1,190	1,865	1,635
5.64	16-QAM ½	1,740	1,475	2,295	2,025
4.23	QPSK	2,000	1,900	2,920	2,610
2.82	QPSK ½	–	2,000	3,000	3,000

Table 8.7 Achievable distance, d, versus supported physical throughput and MCS, for R = 2 and 3km in the presence of sub-channelisation but no sectorization

R_b (Mbps)	MCS	d (m)			
		$R = 2$ km		$R = 3$ km	
		DL	UL	DL	UL
12.27	64-QAM	–	780	–	1,165
11.29	64-QAM 2/3	–	860	–	1,280
8.47	16-QAM	–	1,240	–	1,850
5.64	16-QAM ½	–	1,540	–	2,295
4.23	QPSK	–	1,985	–	2,955
2.82	QPSK ½	–	2,000	–	3,000

Table 8.8 Achievable distance, d, versus supported physical throughput and MCS, for R = 2 and 3 km in the presence of sub-channelisation and sectorization

R_b (Mbps)	MCS	d (m)			
		$R = 2$ km		$R = 3$ km	
		DL	UL	DL	UL
12.27	64-QAM	–	1,460	–	2,095
11.29	64-QAM 2/3	–	1,605	–	2,300
8.47	16-QAM	–	2,000	–	3,000
5.64	16-QAM ½	–	–	–	–
4.23	QPSK	–	–	–	–
2.82	QPSK ½	–	–	–	–

Table 8.9 Percentage of use of each MCS for R = 2 km

R_b (Mbps)	MCS	DL		UL		UL&DL with sub-channelization	
		d (m)	Area (%)	d (m)	Area (%)	d (m)	Area (%)
11.29–12.27	64-QAM	995	24.75	820	16.51	860	18.48
5.64–8.47	16-QAM	1,740	50.94	1,475	37.58	1,540	40.80
2.82–4.23	QPSK	2,000	24.31	2,000	45.61	2,000	40.71

Table 8.10 Percentage of use of each MCS for R = 3 km

d (m)		DL		UL		UL&DL with sub-channelization	
R_b (Mbps)	MCS	d (m)	Area (%)	d (m)	Area (%)	d (m)	Area (%)
11.29–12.27	64-QAM	1,295	18.63	1,130	14.19	1,280	18.20
5.64–8.47	16-QAM	2,295	39.89	2,025	31.37	2,295	40.32
2.82–4.23	QPSK	3,000	41.48	3,000	54.44	3,000	41.48

Table 8.13 presents the results for the average of maximum throughput, $\overline{R_b}$. They are obtained by combining the results for the supported throughput in each coverage ring with the values of the covered area of that crown (which is used as a weight), for both link directions in the presence and absence of sub-channelisation.

Table 8.11 Percentage of use of each MCS in the absence of sub-channelisation but with sectorization

R_b (Mbps)	MCS	$R = 2$ km		$R = 3$ km	
		d (m)	Area (%)	d (m)	Area (%)
11.29–12.27	64-QAM	1,295	41.93	1,500	25.00
5.64–8.47	16-QAM	2,000	58.07	2,695	55.70
2.82–4.23	QPSK	–	–	3,000	19.30

Table 8.12 Percentage of use of each MCS in the presence of sub-channelisation and sectorization

R_b (Mbps)	MCS	$R = 2$ km		$R = 3$ km	
		d (m)	Area (%)	d (m)	Area (%)
11.29–12.27	64-QAM	1,605	64.40	2,300	58.78
5.64–8.47	16-QAM	2,000	35.60	3,000	41.22
2.82–4.23	QPSK	–	–	–	–

Table 8.13 Average of the maximum physical throughput for R = 2 and 3 km

$\overline{R_b}$ (Mbps)	$R = 2$ km			$R = 3$ km		
	No sub-channelisation		With sub-channelisation	No sub-channelisation		With sub channelisation
	DL	UL	UL	DL	UL	UL
Omnidirectional	7.624	6.473	6.803	6.753	5.886	6.751
Sectorial	9.664	9.664	10.808	7.756	7.756	10.605

In the absence of sectorization, while for $R = 2$ km the consideration of sub-channelisation only leads to an increase in UL throughput of 4.8%, from 6.473 to 6.803 Mbps, for $R = 3$ km, the increase achieves 15.1%, from 5.886 to 6.751 Mbps. While for $R = 3$ km the use of sub-channelisation leads to an almost perfect balance between the DL and UL, for $R = 2$ km this improvement does not occur. This can also be verified by comparing the right hand columns of Tables 8.9 and 8.10.

With sectorization, while for $R = 2$ km the consideration of sub-channelisation leads to an increase in throughput in the UL of 11.84%, from 9.664 to 10.808 Mbps, for $R = 3$ km, the respective increase is 36.73%, from 7.756 to 10.605 Mbps. In this case, with the use of sub-channelisation, UL throughput surpasses DL throughput.

In the omnidirectional case, with the use of sub-channelisation, although the noise power decreases the improvement only allows for a perfect balance of the PHY throughputs between the UL and DL for $R = 3$ km (but not for $R = 2$ km).

The use of sectorization reduces the interference, and an improvement on the supported physical throughput of ~59% is obtained for $R = 2$ km (from 6.803 to 10.808 Mbps). However, for $R = 3$ km, as the impact of noise is higher, without the use of sub-channelisation, the improvement only reaches ~32% (from 5.886 to 7.756 Mbps). For $R = 3$ km, only with the use of sub-channelisation and sectorization an improvement of ~57% is achieved (from 6.751 to 10.605 Mbps).

8.3.5 Summary and Conclusions

From the analysis it is clear that both noise and interference present a strong limitation to the performance of fixed WiMAX, mainly for higher level MCSs. As a consequence, with a reuse pattern $K = 7$, cell throughputs near the maximum are only achieved in the UL if sub-channelisation is used together with sectorization.

For lower coverage distances, the use of sectorization alone in the UL allows for a substantial gain in the physical throughput. However, for larger coverage distances, in the absence of sub-channelisation the achieved gain is not comparable with the case where sub-channelisation is used.

These results motivate that future research directions need to be explored to analyse the inclusion of sub-channelisation into the DL, as the IEEE 802.16e standard already supports. Although this will give extra flexibility on resource assignment the extra complexity in the dimensioning process will justify the need for new methodologies, for example, considering scheduling.

Another conclusion that can be extracted from the work is the need to improve the results for the maximum physical throughput in the outer crowns of the cells as this is the zone that suffers the highest interference. The use of relays within fractional reuse schemes, as shown in Fig. 8.27, is being pointed out as a solution for this challenge, and it needs to be investigated.

The presence of relay stations (either fixed or mobile), with limited coverage, will introduce new challenges into the design process, as interference can be mitigated in different ways whilst increasing coverage.

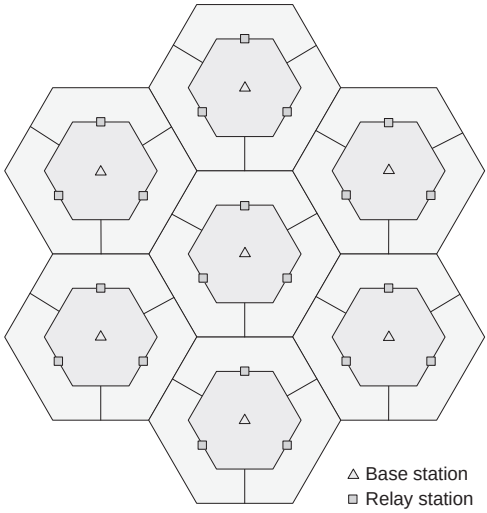

Fig. 8.27 Fractional frequency reuse in a relay-based system where the number of fractional relay stations is 3 (extracted from [14, 15])

8.4 Fixed WiMAX Planning Platforms

8.4.1 Framework and Scenario

Models for the achievable physical throughput, cellular coverage, and frequency reuse are very useful for the automation of cellular planning procedures. Cellular planning is highly dependent on the propagation environment and a careful choice of the placement, height and tilt of the BS transmitter antennas is needed in order to ensure a high percentage of LoS within the cells. As a consequence, the use of Geographic Information System (GIS) is needed to account for the terrain profile.

In the context of the MobileMAN project [16], a cellular fixed WiMAX PtM network [1] was deployed, covering the whole district of Covilhã, and in particular the city area. While the overall cellular structure is mainly dedicated to emergency and security public services, urban micro-cells will support e-learning and e-health services, among others.

Although the district of Covilhã area is 550 km^2, the territorial framework of the frequency band license assigned by ANACOM, the Portuguese regulator, is broader, and includes the whole area under study within the MobileMAN project in Beira Interior, Portugal, where a cellular planning exercise was also performed.

A GIS based WiMAX planning tool was conceived that includes aspects of coverage, frequency reuse, and the impact of classes of services and applications. The tool enables radio and network planning of WiMAX outdoor networks. It relates the geographical data of a given location to the number of BSs needed to cover that location.

This WiMAX platform uses ArcGIS as a working environment [17]. ArcGIS allowed the development of the toolbar that works as a base for network planning. The radio characteristics of the system are studied, including the link budget, the radio capacity, and the definition of the radio propagation models.

Although our tool does consider adaptive MCSs it did not include the functionality of distinguishing among different MCSs in the graphical presentation of the results, that is, it does not display different maps for each MCS. It is therefore worthwhile to explore the functionalities of commercially available tools. The choice was WinpropTM from AWE, which considers the information coming from the digital terrain profile (as our tool does) but displays the several different MCSs on different maps.

8.4.2 Wireless Planning Tool

8.4.2.1 Functionalities and Potentialities

The planning tool is made available as a toolbar in ArcGIS that allows for the user to choose several parameters, from the number of base stations to the number of

users, allowing for network operation in different environments, providing important similarities with real-life situations. The inputs of the tool are the file with the map, including the elevation of the terrain, in digital format, the total coverage area, the most probable position of SSs, as well as the type of applications.

The options included into the ArcGIS toolbar are accessed via buttons, Fig. 8.28, and include the following WiMAX planning functionalities:

- *Definition of urban zones* – With this button urban zones are defined for BSs not operating at the maximum transmitter power since, for these sites, as the user density is much higher than in rural areas, the limitation is the system capacity instead of the radio coverage. Figure 8.29 presents an example of the urban zone of Covilhã over the Digital Map Terrain (DMT).
- *Equipment* – There are two buttons that deal with the WiMAX equipment to be used. The first enables to choose the type of equipment while the second enables the visualization of the equipment data. The equipment list may include items either from a manufacturer available on the market, or customized by the user definitions. In the former case, it is possible to define the bandwidth, frequency, and type of antenna. In the latter, the planner may define all the parameters, for example, bandwidth, transmission power, sensitivity, frequency, and type of antenna, Fig. 8.30.

Fig. 8.28 Toolbar on the graphic environment of ArcGIS

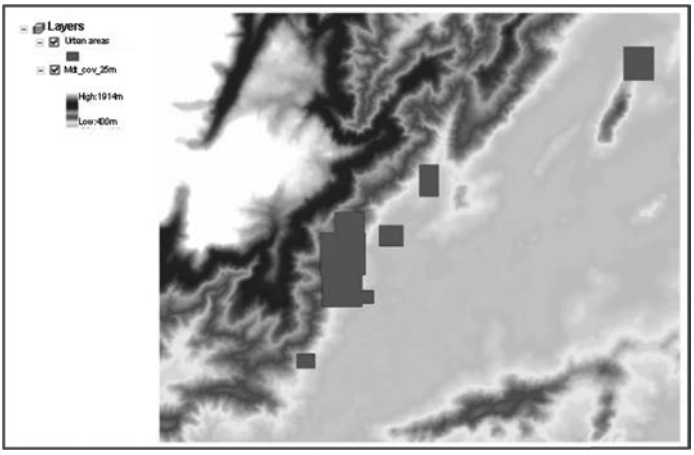

Fig. 8.29 Urban zones in the digital map terrain

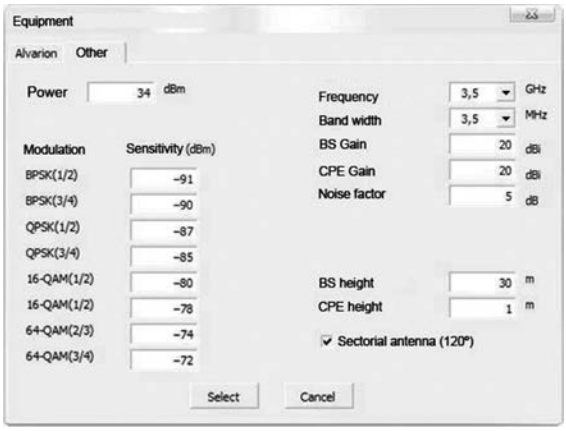

Fig. 8.30 Equipment characteristics: example of a possible choice for the parameters, different from the manufacturer ones

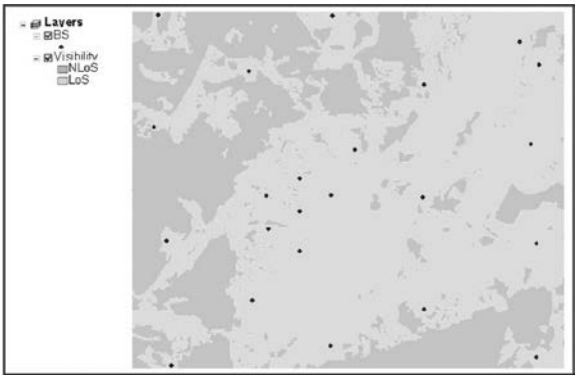

Fig. 8.31 BS positioning and LoS and NLoS areas

- Sites with LoS and NLoS – This option allows for verifying the existence of LoS, and helps to choose the propagation model to be used on each zone of the map, compute the received power and analyze the type of application. This verification is performed by one of the GIS tools, and allows for an optimum verification of the LoS regions originated from each BS, as depicted in Fig. 8.31, example for the district of Covilhã. The actual ArcGIS function used in the tool is Viewshed, a 3D Analyst extension of ArcView.
- Received power and coverage – This functionality creates three different layers. One has the coloured map for each value computed for received power (at each point of the map), depicted in Fig. 8.32. The other shows the values for CNIR. By considering received power and CNIR values, it is possible to check the areas with appropriate coverage and select the spatial option for the capacity. The last layer is a scheme where the different areas covered by each BS can be visualized, as well as the interference areas and the areas with no coverage.

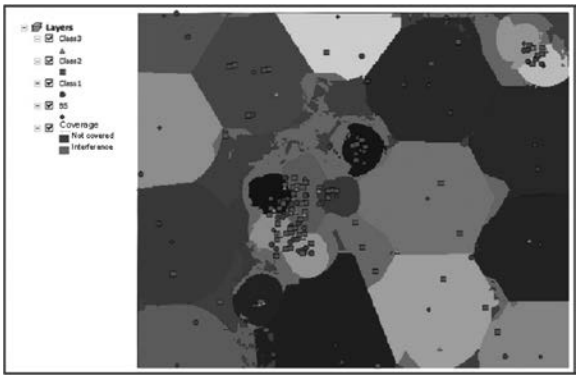

Fig. 8.32 Map with different kind of users (district of Covilhã)

Fig. 8.33 Definition of the distribution of users by classes, their real-time requirements and the density

- *Users* – This button shows a menu to define the percentage of users in each class (e.g., percentages of users with real time services) and the density of users per km^2, as shown in Fig. 8.33. Figure 8.32 shows that these users are then randomly distributed on the map, whilst distinguishing the different classes by different symbols.

The service classes (labelled as one, two and three), distinguish real-time applications at 64, 384, and 2,000 kbps, respectively. A given percentage of users has access to time-based applications (the ones where the time is an intrinsic component of the application), for example, voice or video [18], while others are using non time-based ones. Figure 8.34 depicts some of the results, namely the distribution of users by classes, percentage of area covered and subject to interference, MCSs for each BS, number of users at each cell, throughput and percentage of served users.

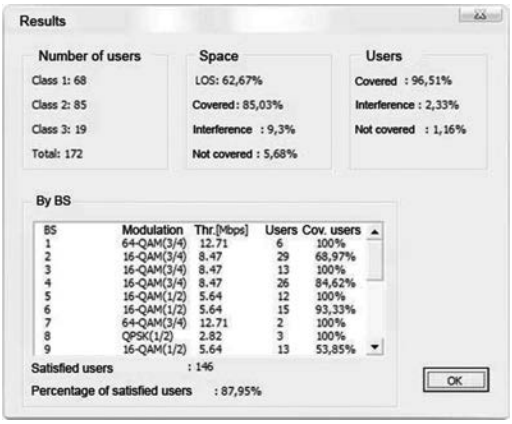

Fig. 8.34 Results arising from the ArcGIS planning tool

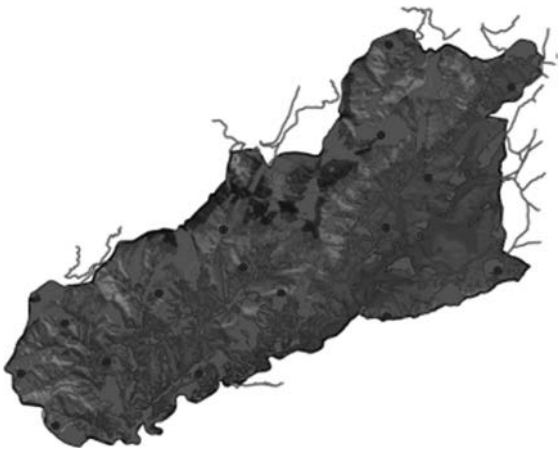

Fig. 8.35 LoS coverage for the district of Covilhã

8.4.2.2 Covilhã Rural and Urban Areas

LoS discovery should be applied for a better cellular planning. GIS functionalities were incorporated into the tool for the choice of the best placement of BSs, including their height.

By considering the use of the modified Friis model, an initial application was made for the district of Covilhã, an area of $\sim$550 km^2. Because this zone is very hilly, cells with coverage distances around 3 km are used, differently from the whole region of Beira Interior, where larger cells were considered. By considering 18 BSs and by using digital terrain models and ArcGIS 9.0, 3D Analyst extension, one obtains LoS coverage in $\sim$70% of the area, Fig. 8.35. In this first case, omnidirectional antennas are mounted on 15 sites (although two of them only cover a 180° sector), while the remaining three sites have two 180° sectorial antennas. It was verified that there is an average of 83% LoS coverage in villages,

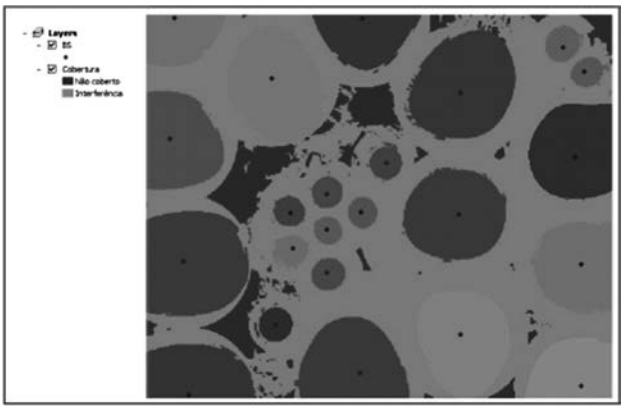

Fig. 8.36 Use of omnidirectional antennas in the district of Covilhã

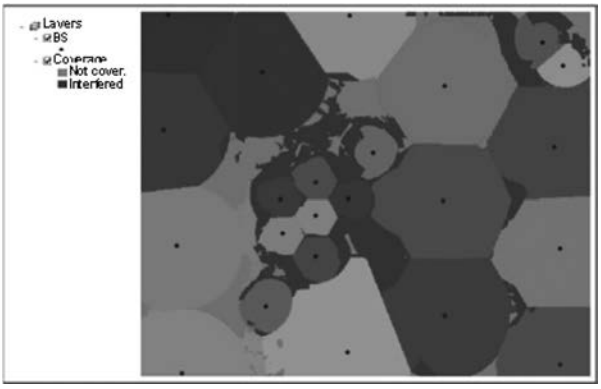

Fig. 8.37 Use of sectorial antennas in the district of Covilhã

towns and cities. This choice guarantees propagation exponents of $\gamma = 2$ in rural areas and $\gamma = 3$ in dense urban areas. Furthermore, main roads on the access to the mountain are covered with LoS.

Another exercise using the ArcGIS platform, in a broader geographical scope, leads to the results from Figs. 8.36 and 8.37, where micro-cells are overlaid with the macro-cellular structure. The height of BS antennas is 30 m, and slightly higher antenna gains are considered compared to the experimental setup. Besides, the transmitter power in urban areas is $\sim$18 dB lower than in rural areas. The SUI-C model was considered in this second case. A comparison between the use of omnidirectional and tri-sectorial cells is performed. In terms of interference mitigation, the advantage of using sectorial antennas is clear. From Table 8.14 one can observe that, with sectorial antennas, the area of interference is reduced from 42%, in the omnidirectional case, down to 9.3%, while the covered area (without interference) increases from 52.3% to 85.0%.

Table 8.14 Coverage and interference areas for the district of Covilhã

Type of Antenna	Coverage area (%)		Non-covered Area (%)
	Without interference	With interference (%)	
Omnidirectional	52.3	42.0	5.7
Sectorial	85.0	9.3	5.7

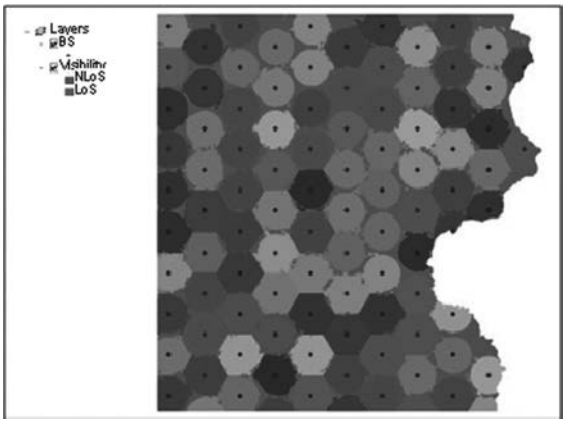

Fig. 8.38 Cellular coverage using sectorial antennas in the whole region of Beira interior

8.4.2.3 Region of Beira Interior

For the WiMAX cellular coverage of the whole region of Beira Interior, a zone with an area of approximately 5,760 km^2 was considered while exploring many combinations for the placement of BSs and types of antennas. One specific exercise compares the use of omnidirectional antennas with the use of sectorial ones over the whole region (Fig. 8.38). The advantages of using the latter in terms of interference mitigation are clear because the area of interference is reduced by 36.1%, from 36.4% to 0.3% while the covered area increases from 50.8% to 86.9%.

Finally, it is worthwhile to note that, as the SUI model is pessimistic in terms of propagation, the results for coverage are appropriate from an engineering perspective, as they represent a worst-case situation. However, results for interference would be worse if a more optimistic model was used for propagation at 3.5 GHz.

A strong need of using sectorial antennas is verified. Sectorial cells guarantee an adequate coverage and interference mitigation for several terrain types and environments, including hilly terrains.

In the particular case of our experiments, optimal planning for the integration of WiMAX and Wi-Fi technologies enables real technical conditions to make the interoperability of these HSF networks available to the students of the Health Science Faculty of University of Beira Interior, where the demonstrator is placed. It provides excellent theoretical, laboratorial, simulation and practical lessons

through multimedia and IP communications, for example, videoconference, voice over IP, and communication of high resolution video/image with the support of terminal mobility, a must for the practice and teaching of medicine. As a final note it is important to mention that these technologies are very attractive in economic terms, when compared to legacy network technologies.

8.4.3 Results with Adaptive Modulation and Coding Schemes

8.4.3.1 Scenario

In the cellular planning exercises with the Winprop^{TM} tool, the geographical scope and the location of BSs were the same as previously considered in Fig. 8.35. However, in this case, 18 tri-sectorial BSs are considered in the district of Covilhã, which corresponds to a total 54 sectors, Fig. 8.39.

Winprop^{TM} enables to present different maps distinguishing each MCS. It also facilitates to explore other propagation models [8], for example, the dominant path loss one, and actual antenna pattern characteristics (from a file with the manufacturer characteristics).

In this part of the work, one considers the parameters from the WiMAX BreezeMAX Alvarion equipment [9], and the frequency bands assigned by ANACOM. The BreezeMAX 3,000 equipment is the Alvarion WiMAX platform for the 3–4 GHz licensed bands. Table 8.15 shows the parameters used in the planning.

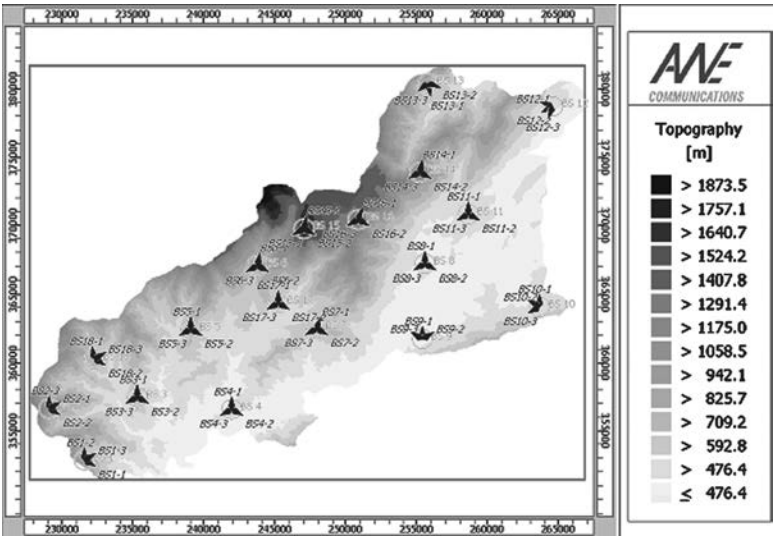

Fig. 8.39 Topography of the district of Covilhã covered with 18 base stations

Table 8.15 Parameters for the planning

Air interface	IEEE 802.16-2004
Number of cell	18
Number of sector per cell	3
Operation frequency	3.5 GHz
Duplexing mode	FDD
Multiple access technique	TDMA
Bandwidth	3.5 MHz
DL/UL separation	100 MHz
Antenna pattern	WiMAX 3500 MHz 120°
BSs height	Several, according to the topography
SS height	1.5 m
Maximum BS output power	43 dBm (19.95 W)
BS antenna gain	15.3 dBi
SS antenna gain	−1 dBi
BS Noise Figure	4 dB
SS Noise Figure	7 dB
Propagation model	Dominant path loss

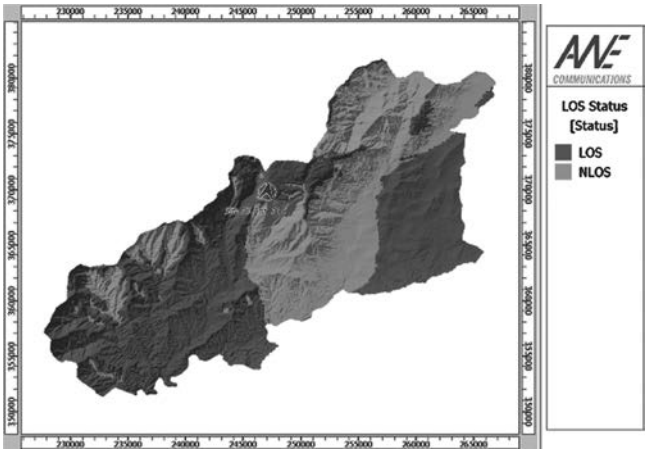

Fig. 8.40 Zones with LoS to BS15

8.4.3.2 Propagation in the District of Covilhã

As an example, Fig. 8.40 presents the LoS regions seen from BS 15 in red while the NLoS regions are presented in green. BS15 is located at the following coordinates: $X = 247{,}000$ m, $Y = 369{,}700$ m (whose reference is a point on the sea near Sagres Point in the south of Portugal), the one assumed by the Portuguese Army Surveying Institute.

The altitude for BS 15 is 1758 m, near the highest point in Portugal continental, the Torre (1993 m), and the antenna tower height is 20 m. One verifies that there is

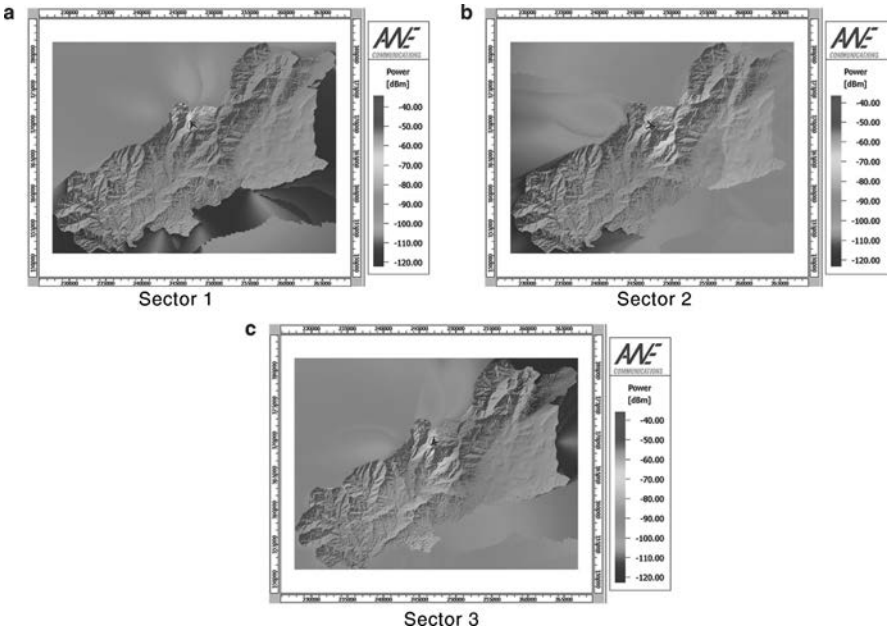

Fig. 8.41 Prediction for the received power for BS15

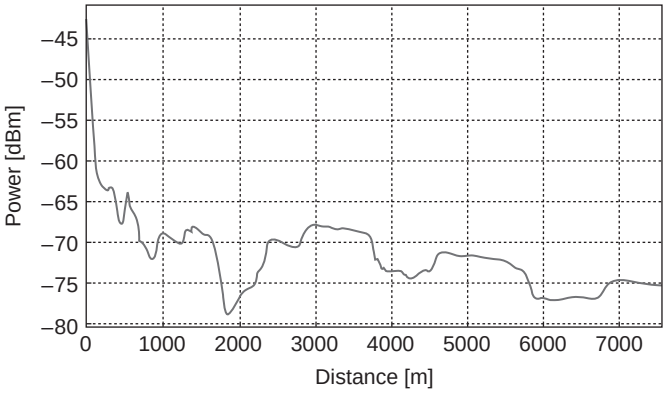

Fig. 8.42 Curve for the received power versus the distance (extracted from the Winprop^{TM} tool)

LoS to the highest regions of the district of Covilhã, and there only is NLoS to the down region, near the city of Covilhã.

Figure 8.41 shows a prediction of the received power at each of the three sectors of BS15. Figure 8.42 is also extracted from the Winprop^{TM} tool in an actual case and helps to analyse the variation of the received power with the distance. The arrow represents the orientation of the sector.

Table 8.16 Correspondence between the MCSs, CNIR and transmission modes

ID	MCS	$CNIR_{min}$ (dB)	Physical throughput (Mbps)
1	BPSK 1/2	3.3	1.41
2	BPSK 3/4	5.5	2.12
3	QPSK 1/2	6.5	2.82
4	QPSK 3/4	8.9	4.23
5	16-QAM ½	12.2	5.64
6	16-QAM 3/4	15.0	8.47
7	64-QAM 2/3	19.8	11.29
8	64-QAM 3/4	21.0	12.27

8.4.3.3 Influence of the Adaptive Modulation and Coding Scheme

In the dimensioning process, it is important to analyse the spatial dependence of the available MCS on the signal strength. The WiMAX equipment uses eight different MCS with different CNIR thresholds (Table 8.16) corresponding to the values for the sensitivity presented in Table 8.2. Planning and network performance results are based on the predictions for the received power (or attenuation) that occurs for each BS sector.

According to AWE Winprop™ terminology, WiMAX network design is essentially based on the detailed analysis of the spatial predictions for each MCS, for example, *CNIR*, received power at the SS and BS, number of channels. Based on these results, the tool determines the physical throughput in the different geographical zones.

8.4.3.4 Prediction of the Maximum Received Power

The tool defines a so-called maximum received power. Figure 8.43 presents its prediction for the DL for the whole district of Covilhã.

In the results shown in Fig. 8.43 all the BSs are simultaneously considered in the prediction of the maximum received power, leading to the results for the variation of the maximum received power with the distance from Fig. 8.44.

One verifies that the decrease of the maximum received power is much smoother than the variation of the received power itself (represented in Fig. 8.42). Another approach may be to analyse the coverage through the consideration of a threshold for the received power. Figure 8.45 presents this analysis for a received power threshold of −80 dBm. A pixel is red if the power is above the threshold and is green if the power is below the threshold. One verifies that with the 18 sectorial BSs a high percentage of coverage is obtained.

8.4.3.5 Prediction of the Maximum Physical Throughput in the DL

Figure 8.46 presents the Prediction of the PHY Throughput in the DL in the whole area covered by the WiMAX network. These results can be analyzed to decide

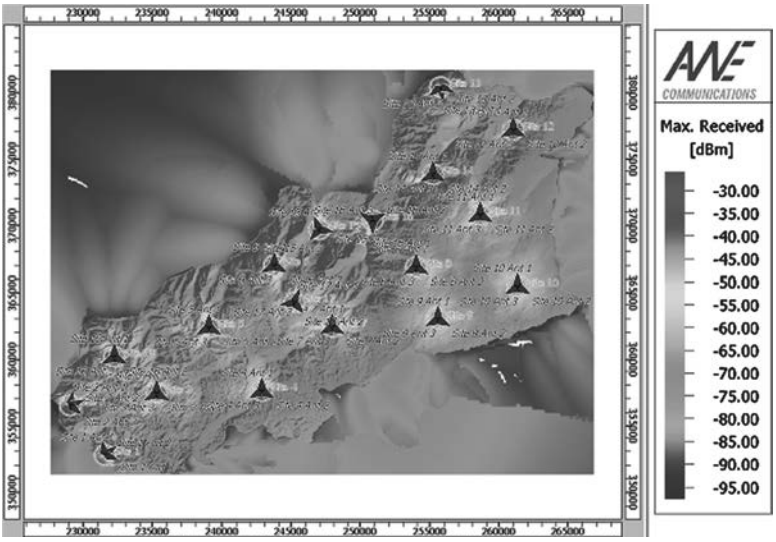

Fig. 8.43 Prediction for the maximum received power in the DL

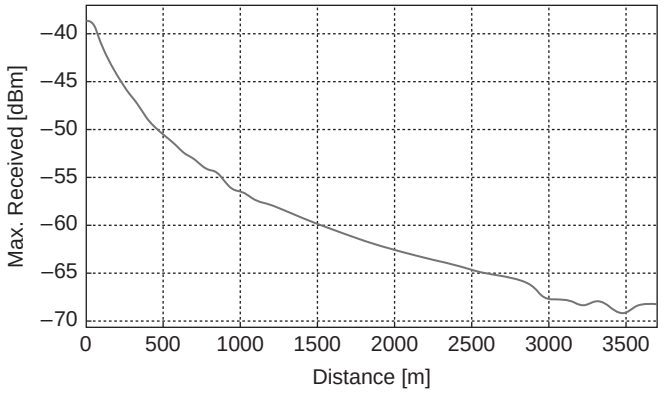

Fig. 8.44 Curve for the prediction for the maximum received power as a function of the distance (extracted from the Winprop™ tool)

where to expect the maximum and the minimum bit rate. For the SSs closer to the BS, an higher order modulation, that is, 64-QAM, is used, whose corresponding bit rate is 12.27 Mbps. For the users located further away, at a medium distance (still not far away from the BS), the 16-QAM modulation is used, and the bit rate is 8.47 Mbps.

For the most distant users, near the cell boundary, QPSK or BPSK modulations are used (supporting data rates of 4.23 and 2.12 Mbps, respectively). This means that, as expected, the farthest the SS is from the BS the lowest is the physical

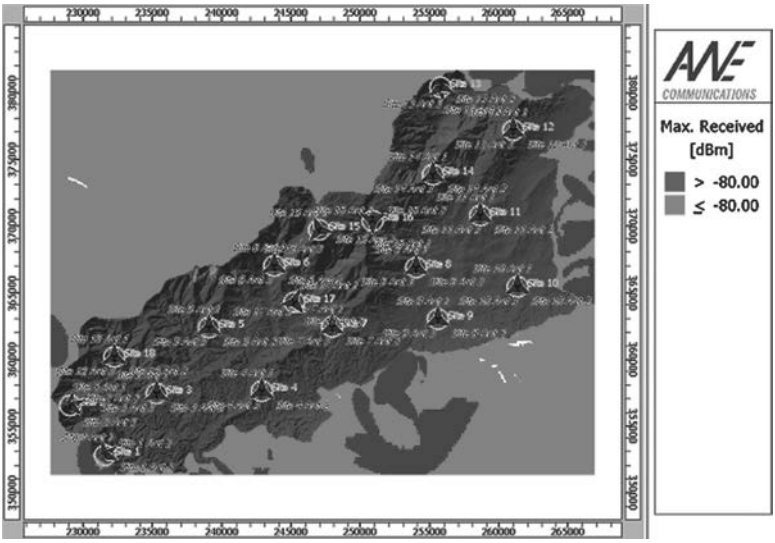

Fig. 8.45 Coverage by considering a threshold for the maximum received power

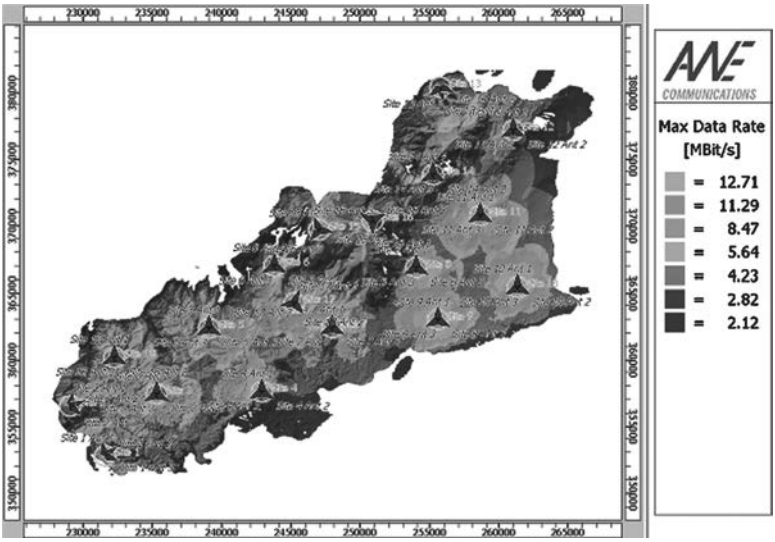

Fig. 8.46 Prediction of the maximum reachable PHY throughput in the DL

throughput. To better interpret these results, it is important to analyze the charts from Figs. 8.47, 8.48, and 8.49, which represent the maximum physical throughput versus the distance, the histogram of the maximum physical throughput, and the cumulative probability for the physical throughput, respectively.

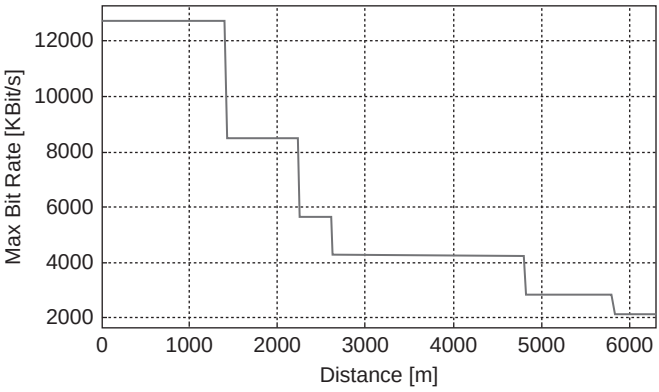

Fig. 8.47 Maximum physical throughput versus the distance (extracted from Winprop^{TM})

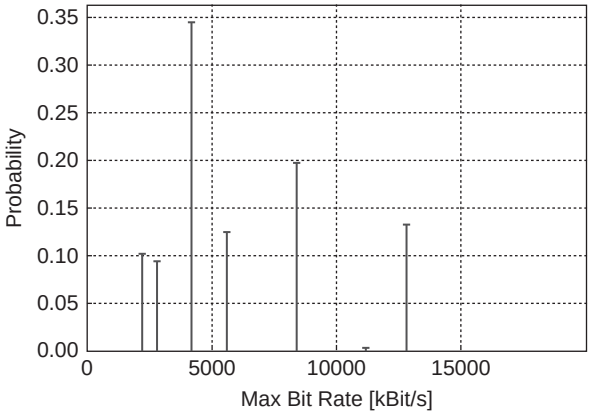

Fig. 8.48 Histogram for the maximum bit physical throughput, R_b (extracted from Winprop^{TM})

By assuming ideal propagation conditions, for distances up to 1.5 km, WiMAX links support the highest order modulation, which corresponds to bit rates that vary between 11.29 and 12.27 Mbps. Then, for distances up to 2.7 km, the order of modulation are the medium ones (bit rates from 5.64 to 8.47 Mbps) while for distances of approximately 6 km one only achieves the lowest order modulations, with bit rates varying from 1.41 to 4.23 Mbps. From Fig. 8.48 one concludes that the MCS mostly used is QPSK (4.23 Mbps), in approximately 35% of the cases, followed by the medium order modulation, 16-QAM (8.47 Mbps), in more than 20% of the cases.

The highest order modulation is used with a frequency of 15%. Figure 8.49 represents the cumulative effect of the results from Fig. 8.48.

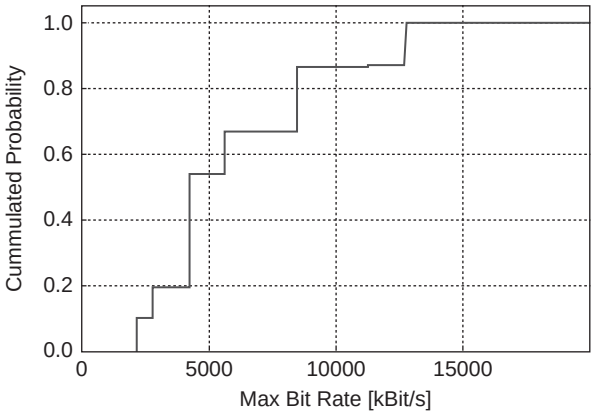

Fig. 8.49 Cumulative histogram for the different supported maximum physical throughput (extracted from Winprop^{TM})

8.4.3.6 Prediction of "Best Server" Cells

In the representation of the "best server" each pixel (representing the SSs) is assigned to a BS sector, more precisely to the carrier assigned to the respective sector, by choosing different colours. As sectorial antennas are used, an aperture angle is defined to each sector antenna. If the pixel is within the range of two different apertures, the assignment is performed to the sector/BS with the lowest associated distance. Figures 8.50 and 8.51 present the maps with the predictions for the "best server" for each MCS.

When the MCS level increases, the area of the "best server" cell/sector decreases as it is only possible to use the highest order MCSs in the regions closest to the BSs. The tool is also able to represent the number of received carriers and of received channels (number of carrier multiplied by the number of time slots). A carrier is received if the received power in a SS is above a pre-defined threshold. The number of received carriers is important to address handover issues, as it is easy to identify the number of different solutions to perform handover. However, as the fixed WiMAX does not support handover the results are not presented.

8.4.3.7 *Carrier-to-Noise-plus-Interference Ratio* in the DL

Maps with the prediction of *CNIR* (or *SNIR*, signal-to-noise-plus-interference ratio) in the DL are also individually produced for each MCS, Fig. 8.52. If the received *CNIR* is below the threshold established to each MCS the pixel is transparently filled; otherwise, it is filled with the colour represented on the scale.

The Winprop^{TM} tool does not consider the UL. Although the results for the UL are generally less favourable, the use of sub-channelisation may allow for overcoming these coverage limitations, as previously discussed.

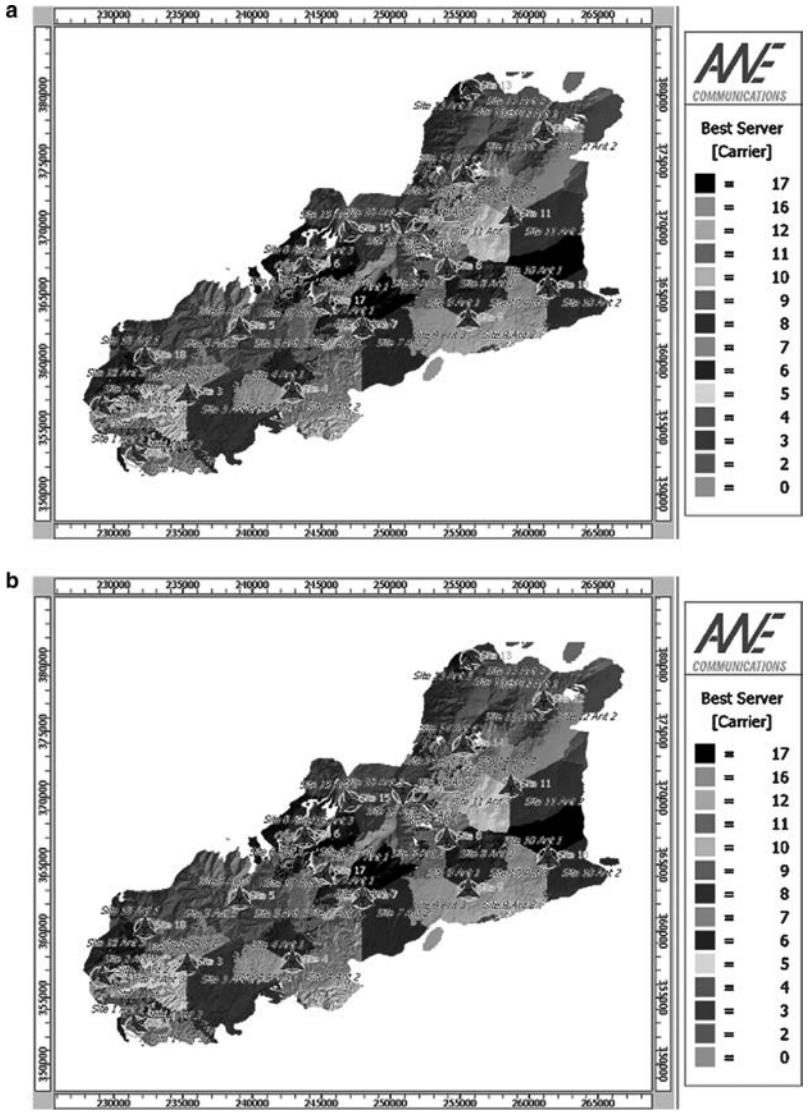

Fig. 8.50 Maps with the "best server" sectors for (**a**) BPSK ½ and (**b**) BPSK

8.4.4 Summary and Conclusions

Two different approaches were considered for cellular planning in the district of Covilhã. On the one hand, one considered a GIS based WiMAX planning tool conceived by considering coverage issues, frequency reuse, the impact of the

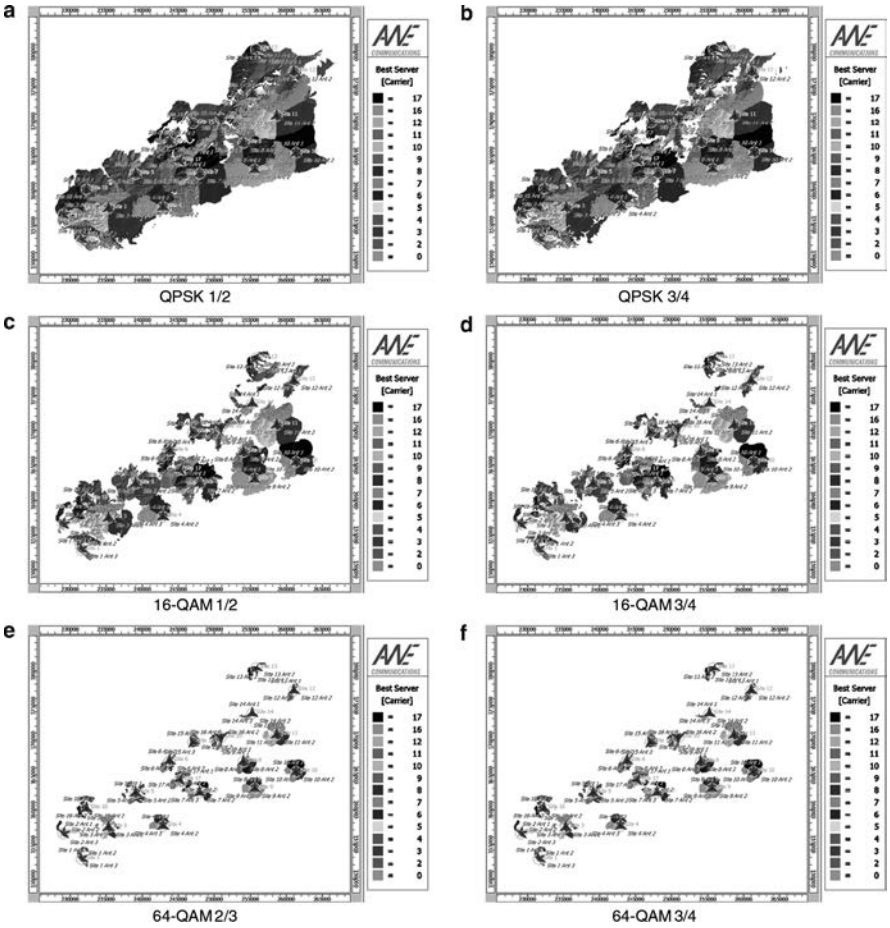

Fig. 8.51 Maps with the "best server" sectors for the remaining MCS

different classes of service. On the other, as adaptive MCS are considered Winprop™ was used.

The GIS functionalities allow for appropriately adjusting azimuth and tilt of antennas. This cellular planning exercises confirm the results theoretical analysis, where different crowns are achieved for the coverage with each MCS (corresponding to a given range of values for *SNIR*), and also for the maximum PHY throughput and for the "best server" cells. The benefit of using sectorization was also demonstrated.

Cost/revenue optimisation will allow for finding the optima for the planning. There are fixed costs (e.g., spectrum licenses), plus costs proportional to the number of cells, and the cost proportional to the number of "transceivers". Typically, total costs depend on the size of the cells and on the reuse pattern. Revenues depend on the supported throughput (which also depends on the size of the cells and on the

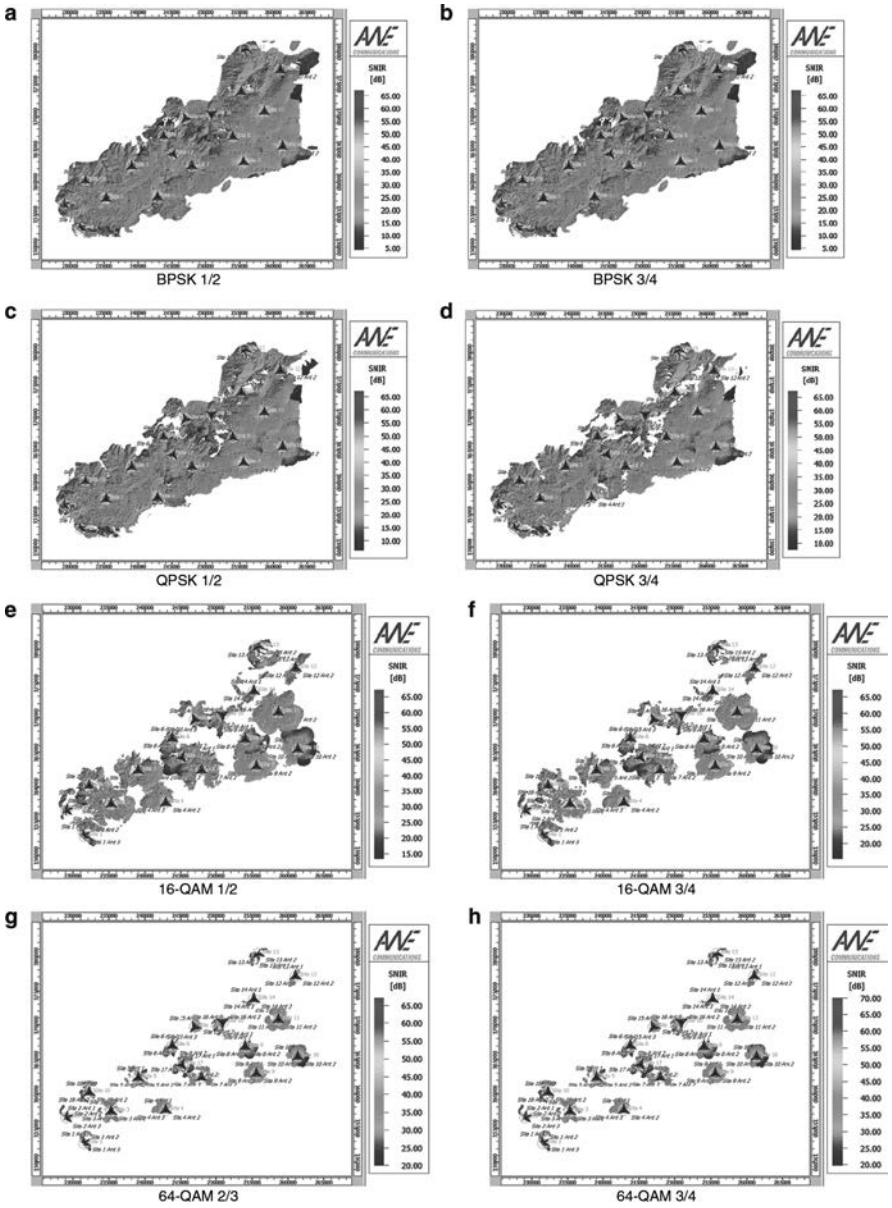

Fig. 8.52 Maps with the *SNIR* prediction in the DL

reuse pattern). They depend on prices and will be very sensitive to the number of supported users.

Regarding the profit, the absolute profit is usually proportional to the supported "traffic" (e.g., per km^2). The profit in percentage is, however, proportional to the

"spectral efficiency", and companies usually want to maximize the profit in percentage [19]. Further work is needed to seek for optimum coverage distances in different reuse configurations accounting for cost-benefit optimisation.

8.5 Conclusions

In this Chapter, one started by considering a PtM demonstrator for fixed WiMAX that allowed for extracting measurements for cellular coverage in the suburban area of Covilhã, Portugal. For this zone, and for some ranges for the distances, by using a curve fitting approach one concluded that the modified Friis model can be used with a propagation exponent $\gamma = 3$. From the analysis of the results, one can also conclude that the Stanford University Interim model can be considered (mainly SUI-C but also SUI-B), as the mean square error is kept under reasonable values.

Then, an analytical approach was used to determine the trade-offs between the coverage distance and interference minimisation whilst increasing system capacity. From the analysis, it is clear that both noise and interference present strong limitations to the performance of fixed WiMAX, mainly for higher MCS levels. With a reuse pattern $K = 7$, cell throughputs near the maximum are only achieved, in the UL, if sub-channelisation is used together with sectorization. With the use of sub-channelisation alone, although the noise power decreases, the improvement is not so clear.

For the shortest coverage distances, the use of sectorization alone in the UL allows for obtaining a substantial gain in the physical throughput. However, for larger coverage distances, in the absence of sub-channelisation, the achievable gain is not comparable with the case where sub-channelisation is used.

In general terms, the use of sectorization in fixed WiMAX enables to reduce the reuse pattern while considering sub-channelisation allows for improvement on the coverage. The reduction of the reuse pattern directly corresponds to an increase in the system capacity but the improvement in the coverage range (through sub-channelisation) can also allow for an improvement in UL system capacity, as adaptive MCS are used.

The need to improve the results for the maximum achievable throughput in the outer coverage rings of the cells, as this is the zone that suffers the highest interference, motivates future research directions, for example, by using relays within fractional reuse schemes. The presence of relay stations (either fixed or mobile), with limited coverage, will introduce new challenges into the design process, as interference can be mitigated in different ways whilst increasing coverage (e.g., by decreasing the transmitter power or by using advanced scheduling techniques).

One interesting aspect which is left for further study is on the dependence of the results on the propagation exponent, γ. For example, if the propagation exponent decreases, for example, to $\gamma = 2.3$, the value of the asymptote for the coverage area

will increase and the asymptotic value for the reuse factor, r_{cc}, will increase, corresponding to a reduction on system capacity for each MCS.

Two different approaches were considered for graphical cellular planning, and the district of Covilhã was considered as a case study. On the one hand, one considered a GIS based WiMAX planning tool conceived by considering coverage issues, frequency reuse, and the impact of the different classes of service. On the other, Winprop™ was used as it distinguishes among different MCS in the graphical presentation of the results. Both tools consider the information coming from the digital terrain profile. The GIS functionalities allow for appropriately adjusting azimuth and tilt of antennas. This cellular planning exercises confirm the results of theoretical analysis, where different crowns are achieved for the coverage with each MCS (corresponding to a given range of values for *SNIR*), for the maximum physical throughput, and for the "best server" cells.

The frequency radio resources should be considered as the most valuable resource during the planning of wireless broadband access networks. As a rule, spectral efficiency needs to be optimized by using several advanced techniques, corresponding to an optimization from the cost-benefit point of view.

Acknowledgement This work was partially funded by MobileMAN (Mobile IP for Broadband Wireless Metropolitan Area Network), an internal project from Instituto de Telecomunicações/ Laboratório Associado, by CROSSNET (Portuguese Foundation for Science and Technology POSC project with FEDER funding), by "Projecto de Re-equipamento Científico" REEQ/1201/ EEI/ 2005 (a Portuguese Foundation for Science and Technology project), and by the Marie Curie Intra-European Fellowship OPTIMOBILE (Cross-layer Optimization for the Coexistence of Mobile and Wireless Networks Beyond 3G, FP7-PEOPLE-2007-2-1-IEF). The authors acknowledge the fruitful contributions on ArcGIS tools from Engº José Romão, Engº José Riscado and Prof. Victor Cavaleiro from STIG-UBI, and to the final year project students Hugo Carneiro, Jorge Oliveira, Dany Santos and Rui Marcos.

References

1. IEEE, Draft IEEE Standard for Local and Metropolitan Area Networks – Part 16: Air Interface for Fixed Broadband Wireless Access Systems, IEEE 802.16-REVd/D5, The Institute of Electrical and Electronics Engineers, New York, USA, May 2004
2. IEEE, Draft IEEE Standard for Local and Metropolitan Area Networks – Part 16: Air Interface for Fixed Broadband Wireless Access Systems – Amendment for Physical and Medium Access Control Layers for Combined Fixed and Mobile Operation in Licensed Bands, IEEE 802.16e/D9, The Institute of Electrical and Electronics Engineers, New York, USA, June 2005
3. http://www.awe-communications.com
4. V. Erceg et al., An empirically based path loss model for wireless channels in suburban environments. IEEE J. Select. Areas Commun. **17**(7), 1205–1211 (July 1999)
5. IEEE 802.16 Working Group, Channels models for fixed wireless applications, Document 802.16.3c-01/29r4 (July 2001)
6. K. Hari, Interim Channel Models for G2 MMDS Fixed Wireless Applications, in *IEEE 802 plenary meeting*, Tampa, USA, Sept 2000. www.ieee802.org/16/tg3/contrib/802163c-00_49r2.pdf (March 2010)

7. H.R. Anderson, *Fixed Broadband Wireless Systems Design* (Wiley, Chichester, West Sussex, UK, 2003)
8. R. Wahl, O. Stäbler, G. Wölfle, Propagation model and network simulator for stationary and nomadic WiMAX networks, in *Proceedings of IEEE VTC 2007 Fall – IEEE 66th Vehicular Technology Conference*, Baltimore, MD, USA, Sept 2007
9. http://www.alvarion.com
10. T.S. Rappaport, *Wireless Communications: Principles and Practice* (Prentice Hall, Upper Saddle River, NJ, 2002)
11. F.J. Velez, L.M. Correia, J.M. Brázio, Frequency reuse and system capacity in mobile broadband systems: comparison between the 40 and 60 GHz bands. Wireless Pers. Commun. **19**(1), 1–24 (Aug 2001)
12. F.J. Velez, V. Carvalho, D. Santos, R.P. Marcos, R. Costa, P. Sebastião, A. Rodrigues, Planning of an IEEE 802.16e network for emergency and safety services, in *Proceedings of 3G 2005 – 6th IEE International Conference on 3G Mobile Communication Technologies*, London, UK, Oct 2005
13. F.J. Velez, Aspects of cellular planning in Mobile Broadband Systems, PhD thesis, Instituto Superior Técnico, Universidade Técnica de Lisboa, Lisbon, Portugal (Dec 2000)
14. K.A. Rizvi, Young sun, D. Basgeet, Z. Fan, P. Strauch, Fractional frequency reuse for IEEE 802.16j relaying mode. IEEE C80216j-06_223, IEEE (Nov 2006)
15. http://www.wimaxforum.org/documents/downloads
16. http://www.e-projects.ubi.pt/mobileman
17. H. Carneiro, J. Oliveira, A. Rodrigues, P. Sebastião, Software planning tool for WiMAX networks, in *Proceedings of Conftele' 2007 – 7th Conference on Telecommunications*, Peniche, Portugal (May 2007)
18. F.J. Velez, L.M. Correia, Mobile broadband services: classification, characterisation and deployment scenarios. IEEE Commun. Mag. **40**(4), 142–150 (Apr 2002)
19. F.J. Velez, L.M. Correia, Optimisation of mobile broadband multi-service systems based in economic aspects. Wireless Netw. **9**(5), 525–533 (Sept 2003)